FLT3L-dependent dendritic cells control tumor immunity by modulating Treg and NK cell homeostasis

Paul Régnier, Mathias Vetillard, Adèle Bansard, Eméranne Pierre, Xinyue Li, Nicolas Cagnard, Emmanuel L Gautier, Pierre Guermonprez, Bénédicte Manoury, Katrina Podsypanina, et al.

Cell Reports
Medicine

Article

FLT3L-dependent dendritic cells control tumor immunity by modulating Treg and NK cell homeostasis

Graphical abstract

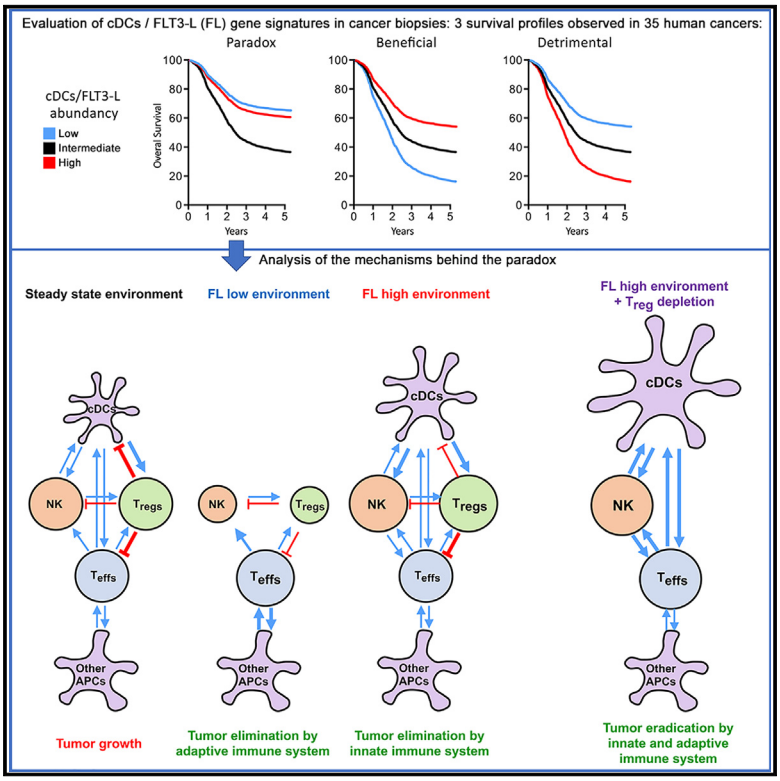

Highlights

- Deficit or excess of Flt3L and DCs paradoxically extends life in mice and humans with cancer
- Low DCs restrict tumor growth via adaptive immunity, high DCs via innate immunity
- Increased Flt3L and Treg inhibition synergize to improve cancer survival in mice/humans
- Flt3-L, cDCs, and pDCs gene signatures in the biopsies of cancer patients predict survival

Authors

Paul Régnier, Mathias Vetillard, Adèle Bansard, ..., Bénédicte Manoury, Katrina Podsypanina, Guillaume Darrasse-Jèze

Correspondence

guillaume.darrasse-jeze@inserm.fr

In brief

Régnier et al. examine the role of Flt3L-dependent dendritic cells in cancer and show that both their deficit or excess can paradoxically extend life in mice and humans. They identify their beneficial/adverse/paradoxic roles in 35 human cancers and demonstrate that Treg inhibition and Flt3L synergize to improve cancer survival.

Régnier et al., 2023, Cell Reports Medicine *4*, 101256
December 19, 2023
https://doi.org/10.1016/j.xcrm.2023.101256

CellPress

Cell Reports Medicine

CellPress
OPEN ACCESS

Article

FLT3L-dependent dendritic cells control tumor immunity by modulating Treg and NK cell homeostasis

Paul Régnier,[1,2,3] Mathias Vetillard,[4,5] Adèle Bansard,[1,6] Eméranne Pierre,[6] Xinyue Li,[2] Nicolas Cagnard,[7] Emmanuel L. Gautier,[8] Pierre Guermonprez,[4,5] Bénédicte Manoury,[1] Katrina Podsypanina,[1,9] and Guillaume Darrasse-Jèze[1,2,6,10,*]

[1]Institut Necker Enfants Malades, INSERM U1151, CNRS UMR-8253, Université Paris Cité, Paris, France
[2]Sorbonne Université, INSERM, UMR_S959, Immunology-Immunopathology-Immunotherapy, Paris, France
[3]AP-HP, Groupe Hospitalier Pitié-Salpêtrière, Department of Internal Medicine and Clinical Immunology, DMU3ID, Paris, France
[4]Université de Paris Cité, Centre for Inflammation Research, INSERM U1149, CNRS ERL8252, Paris, France
[5]Dendritic Cells and Adaptive Immunity Unit, Institut Pasteur, Paris, France
[6]Université Paris Cité, Faculté de Médecine, Paris, France
[7]Structure Fédérative de Recherche Necker, Université Paris Descartes, Paris, France
[8]Inserm, UMR_S1166, Sorbonne Université, Hôpital Pitié-Salpêtrière, Paris, France
[9]Institut Curie, PSL Research University, CNRS, Sorbonne Université, UMR3664, Paris, France
[10]Lead contact
*Correspondence: guillaume.darrasse-jeze@inserm.fr
https://doi.org/10.1016/j.xcrm.2023.101256

SUMMARY

FLT3-L-dependent classical dendritic cells (cDCs) recruit anti-tumor and tumor-protecting lymphocytes. We evaluate cancer growth in mice with low, normal, or high levels of cDCs. Paradoxically, both low or high numbers of cDCs improve survival in mice with melanoma. In low cDC context, tumors are restrained by the adaptive immune system through influx of effector T cells and depletion of Tregs and NK cells. High cDC numbers favor the innate anti-tumor response, with massive recruitment of activated NK cells, despite high Treg infiltration. Anti CTLA-4 but not anti PD-1 therapy synergizes with FLT3-L therapy in the cDC^{Hi} but not in the cDC^{Lo} context. A combination of cDC boost and Treg depletion dramatically improves survival of tumor-bearing mice. Transcriptomic data confirm the paradoxical effect of cDC levels on survival in several human tumor types. cDC^{Hi}-$Treg^{Lo}$ state in such patients predicts best survival. Modulating cDC numbers via FLT3 signaling may have therapeutic potential in human cancer.

INTRODUCTION

FLT3-L (FL) is a transmembrane/soluble molecule initially identified as a growth factor[1–3] stimulating the differentiation and division of early hematopoietic progenitor cells such as LSK ($Lin^-Sca1^+Kit^-$) cells in mice.[4,5] FL is recognized by Flt3 (CD135/Flk2), a tyrosine kinase receptor expressed by several classes of stem/progenitor cells.[6,7] But while FL deficiency affects the frequency of hematopoietic progenitor cells in the bone marrow (BM), it has little effect on mature lymphocytes and myeloid cells in the periphery. Instead, FL deficiency results in an almost complete absence in the periphery of classical dendritic cells (cDCs),[8] a specialized family of $CD11c^{hi}MHC\text{-}II^+Flt3^+zDC/Zbtb46^+$ cells that process and present antigens to lymphocytes for initiation and regulation of immune responses.[9,10] Indeed, FL is essential for the differentiation and proliferation of cDC and plasmacytoid DC (pDC) progenitors in the BM.[7,11–16] FL is also required for the differentiation of pre-CDPs into DC1s, a subset of cDCs cross-presenting antigens to $CD8^+$ T cells (CTLs), and into DC2s, a subset of cDCs more readily priming $CD4^+$ helper T cell (Th) response *in vivo*.[17] Once in lymphoid organs, cDCs may divide,[18] but not in an FL-deficient environment.[2] Excess of FL leads to DC progenitor differentiation, expansion, and migration from the BM to the circulation. FL treatment in human healthy volunteers results in a phenomenal expansion of DC numbers in peripheral blood.[16,19] Thus, FL appears crucial for the differentiation and peripheral homeostasis of cDCs and represents a promising molecule for therapy.[19–21]

In contrast, FL does not directly affect NK cells, as they neither express Flt3 nor respond to FL *in vitro*,[22] and there is no other receptor binding FL in the absence of Flt3.[23] Instead, NK cell homeostasis/survival depends on IL-15.[24–27] DCs can recycle and trans-present IL-15 to neighboring cells via their own IL-15Rα.[28–31] Instructive experiments using diphtheria toxin (DT)-mediated depletion in the $CD11c^{DTR}$ mice suggest that FL effect on NK cell homeostasis is mediated through DCs.[32,33] However, a genetic proof is lacking. Conversely, in the cancer context, NK cells can recruit DCs by producing FL[34] or CCL5 and XCL1[35] at the tumor site.

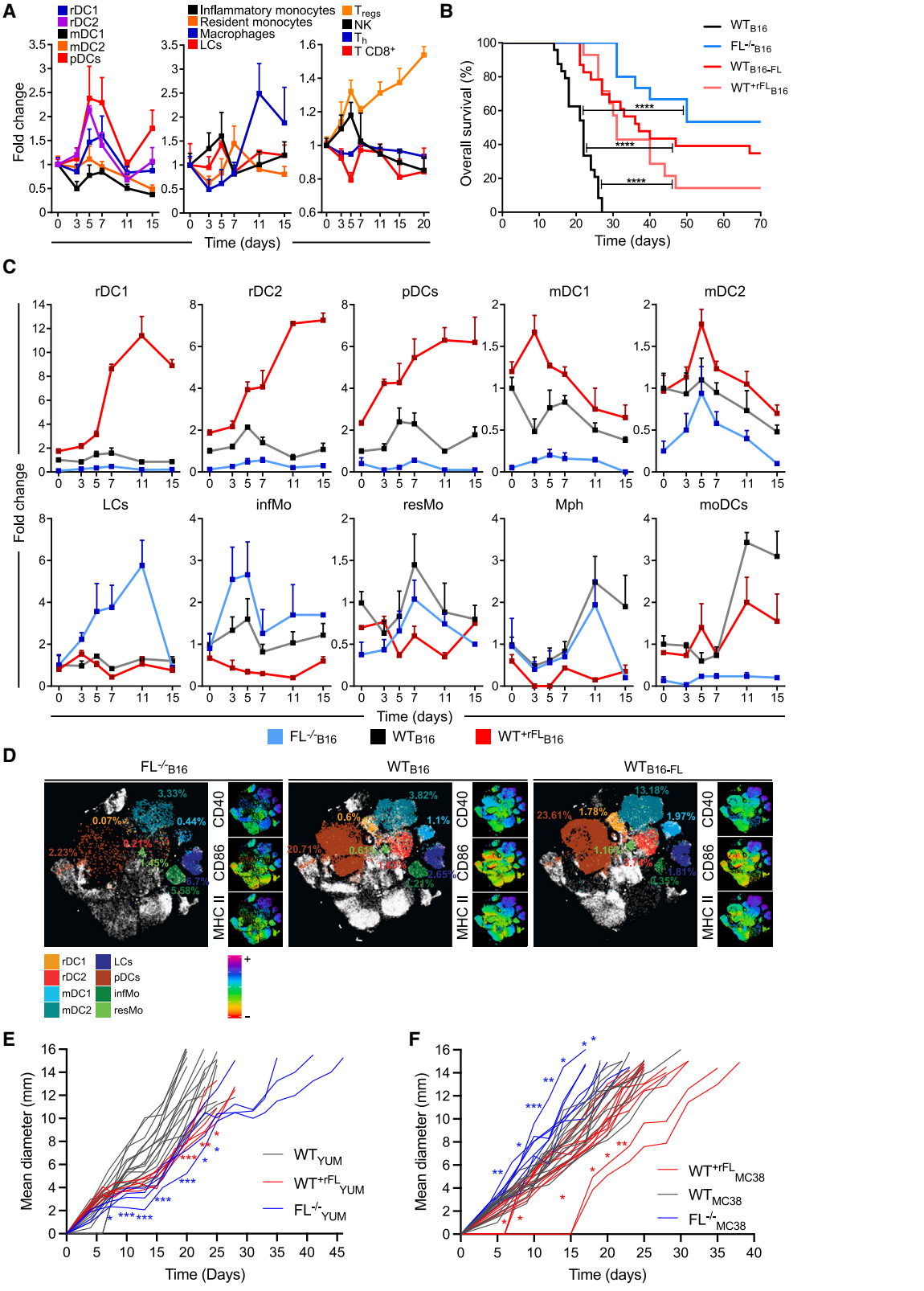

(legend on next page)

The FL-dependent mature cDCs efficiently prime naive T cells for immune response against foreign antigens; they are also required to induce immune tolerance against antigens at the steady state[36–38] and to induce dominant immune tolerance to tumors.[39–41] In cancer, the involvement of FL-dependent and -independent DCs is not straightforward.

Cross-presenting rDC1s (LN- and spleen-resident DC1s) and mDC1s (tissue-to-LN migratory DC1s) promote anti-tumor immune response to cancer[42–45] but are also major DC subsets involved in peripheral Treg (pTreg) induction *in vivo*.[46–51] Dermal cDCs and Langerhans cells (LCs) contribute to the mDC population when they reach the LNs and are also able to generate pTregs[52] that support tumor development,[53,54] complicating the interpretation of their role in cancer. Less is known about the role of DC2 in cancer. DC2 may be suppressive,[55] and rDC2s promote proliferation of tolerogenic thymic-derived Tregs (tTregs) *in vivo*.[46] Yet some studies uncovered an immunostimulatory role for DC2 in cancer in the $Treg^{Lo}$ context[56] and they provide beneficial effect when used for vaccination.[57] pDCs in cancer also have a tolerogenic role in the absence of inflammation and may inhibit NK cells while boosting Treg recruitment.[58–62] In addition, pDC depletion leads to better control of tumor growth, but TLR7 stimulation abrogates their tolerogenic effect and allows them to induce strong anti-tumor responses.[63–66]

The most straightforward way for DCs to mediate tumor tolerance is to stimulate tTregs, the self-specific lymphocyte subset responsible for maintaining self-tolerance and protection against autoimmunity.[67] In many mouse models of cancer, activated/memory self-specific tTregs are quickly recruited in the dLNs and in the tumor site at the early stages of tumor development by recognizing MHC class II-presented self-specific antigens.[40,68–71] Their accumulation leads to generalized suppression of the anti-tumor response through inhibition of $CD4^+$ and $CD8^+$ T cells and NK cells.[40,71,72] Cancer-associated Treg recruitment is also observed in humans[73–78] and may represent a major barrier to effective immunotherapies.[79] Indeed, in several cases, inhibition of Treg suppression enhances anti-tumor immune responses and results in tumor eradication.[72,80–82]

As tumors do not express MHC class II, presentation of tumor antigens to Tregs must be performed by professional APCs. Under physiological conditions, recruitment and survival of Tregs appear to be highly dependent on DC numbers.[83] DC deficiency is indeed associated with depletion of Tregs in humans,[84] leading to auto-immune manifestations.[85] It is possible that accumulation of Tregs in cancer is mediated by a regulatory feedback loop between Tregs and DCs. One way to test this hypothesis is to modify the number of DCs at the time of tumor emergence by modulating levels of FL.

In this study, we evaluated the effect of FL deficiency/overexpression on immune response against highly tolerogenic melanoma in mice. We observed that FL deficiency boosts the adaptive anti-tumor immune response by diminishing Treg numbers and function, while FL overexpression favors the anti-tumor innate response by increasing NK cell numbers and function in a DC-dependent manner. We validated these findings in several genetic mouse models of DC depletion and carried out a proof-of-principle preclinical study to demonstrate that combination of FL overexpression and Treg depletion can enhance anti-tumor effects and increase survival of melanoma-bearing mice.

Using transcriptomic data of cancer patients, we show that paradoxical FL effect on survival is also evident in some human cancers. More broadly, most studied human cancers display a correlation between Treg, NK cell and FL, cDCs and pDC gene signature expression levels. Thus, FL-dependent DCs control immune response to cancer via Treg and NK cell homeostasis. Our results advocate FL as an important biomarker for anti-cancer immunotherapy decisions.

RESULTS

A paradoxical role for FL in tumor immune response is linked to DCs

To determine when/how different DC subsets and other immune cells participate in early tumor immune response, we examined evolution of immune cell composition in the tumor-draining lymph nodes (dLNs), which are essential for the initiation of tumor rejection or tolerance.[43,86,87] Using C57Bl/6 mice developing melanomas from B16 cells, we collected dLNs at different time points following tumor injection. Using multiparameter flow cytometry (gating strategies available in Figures S1A and S2A), we evaluated the fold change in the proportions of different

Figure 1. FL levels affect DC frequencies and survival of tumor-bearing mice

(A) Tumor appearance drives a transient increase in DC and a sustained increase in Treg frequencies in the dLNs of B16 melanoma-bearing mice (WT_{B16}). Fold change was calculated by dividing the target cell fraction among live $CD3^-CD19^-NK1.1^-$ cells (left/center) or $CD45^+$ live cells (right) in tumor-bearing mice to that in tumor-free mice (n = 5–15 mice per time point).

(B) Kaplan-Meyer plot showing improved overall survival of B16-bearing FL-deficient ($FL^{-/-}{}_{B16}$, blue, n = 17, log rank test difference with W_{B16}: $p < 0.0001$), FL-overexpressing mice ($WT_{B16\text{-}FL}$, red, n = 19, $p < 0.0001$ or $WT^{+rFL}{}_{B16}$, pink, n = 17, $p < 0.0001$) over control animals (WT_{B16}, black, n = 24) (4 experiments pooled).

(C) FL levels modify cDC and pDC dynamics in the dLN during cancer development. Fold change was calculated by dividing the target cells fraction among the $CD3^-CD19^-NK1.1^-$ in $FL^-/^-{}_{B16}$ and $WT^{+rFL}{}_{B16}$ tumor-bearing mice to that in WT_{B16} mice (n = 5–15 per time point). Similar results were obtained in the $WT_{B16\text{-}FL}$ group (not shown).

(D) t-SNE plots of surface and activation marker expression on samples from (C) demonstrate equivalent levels of functional APCs in the dLNs in the three groups of mice. Each plot is a concatenation of 3 replicate FCS files. Each dot represents a single cell, colored according to the subset. Percentages indicate subset fraction among live $CD3^-CD19^-NK1.1^-$ cells. The intensities of expression of CD40/CD86/MHC class II are overlaid for each condition (small plots).

(E) Tumor growth is delayed in YUMM1.7-bearing FL-deficient ($FL^{-/-}{}_{YUM}$, blue) and FL-overexpressing mice ($WT^{+rhFL}{}_{YUM}$, red) over control animals (WT_{YUM}, black), n = 4–13 per group (2 experiments pooled).

(F) Tumor growth is delayed in MC38-bearing FL-overexpressing mice ($WT^{+rhFL}{}_{MC38}$, red) over controls (WT_{MC38}, black) but not in FL-deficient ($FL^{-/-}{}_{MC38}$, blue) mice, n = 4–14 per group (3 experiments pooled). Multiple Student's t tests were performed to compare groups. For all tests, *$p < 0.05$, **$p < 0.01$, ***$p < 0.001$, ****$p < 0.0001$.

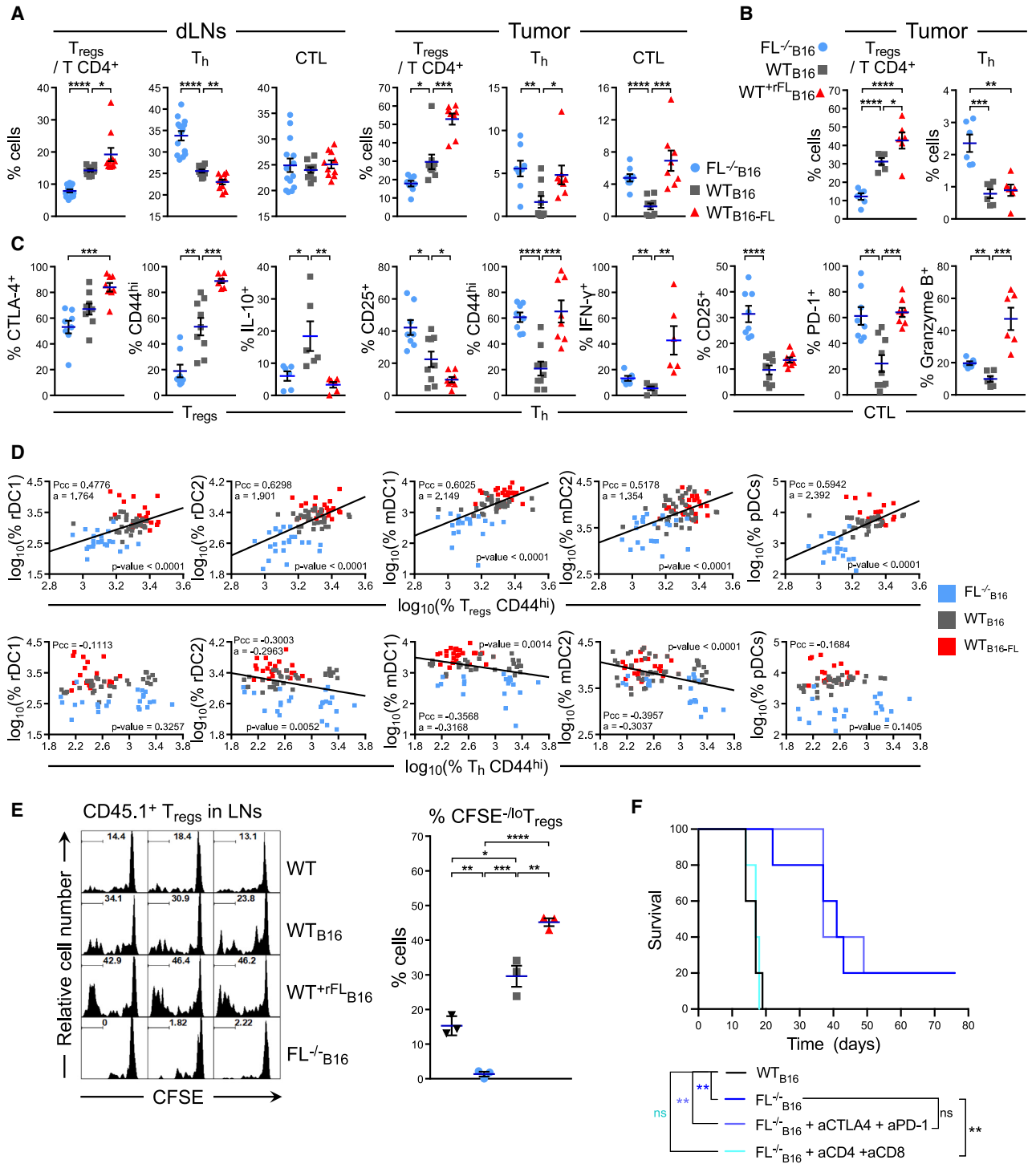

Figure 2. FL levels affect frequencies and activity of Tregs and Teffs cells in tumor and dLN

(A) The T cell compartment of WT_{B16} (black), $FL^{-/-}{}_{B16}$ (green), and $WT_{B16\text{-}FL}$ (red) mice were investigated by flow cytometry. Scatterplots show the frequencies of the indicated cell subsets in the dLNs (n = 10–14 per group) or in the tumor (n = 8–9 per group) at day 11 post-inoculation.

(B) Confirmation of the results in $WT^{+rFL}{}_{B16}$ mice. Scatterplots show the percentages of Tregs and Th cells at day 10 in tumors of WT_{B16} (black), $FL^{-/-}{}_{B16}$ (green), and $WT^{+rFL}{}_{B16}$ (red) mice (n = 6 per group).

(C) Frequencies of tumor-infiltrating cells expressing the indicated activation markers among the cell subsets described in (A) and the percentage of IL-10-, IFN-γ-, and granzyme-B-expressing cells after *ex vivo* restimulation (n = 6 per group).

(legend continued on next page)

immune cell subsets (Figure 1A). The appearance of a tumor reproducibly induces a transient increase of rDC1s, rDC2s, and pDCs, as well as inflammatory monocytes (infMos), which peak at day 5 and then fall back to levels observed in tumor-free mice. Macrophage (Mph) proportions increase later, at day 11. Among lymphoid populations, only Tregs and NK cells mirror the increase in DCs, steadily for Tregs and transiently for NK cells. These results confirm that early tumor development favors DC recruitment in the LNs.[88]

To examine the role of FL-dependent cDCs during tumor development, we evaluated the effect of FL deficiency and overexpression on tumor growth and mouse survival. To model FL deficiency, we used B16 melanoma-bearing $FL^{-/-}$ mice[8] ($FL^{-/-}{}_{B16}$) (see Table S2 for abbreviations). To test the effect of high FL levels, we used mice either bearing B16 tumors overexpressing FL ($WT_{B16\text{-}FL}$),[89] or mice injected with soluble FL during tumor growth ($WT^{+rFL}{}_{B16}$).[90] B16 cells do not express the Flt3 receptor (Figure S1D).

Paradoxically, groups deficient for FL and those with an excess of FL display extended survival (Figure 1B) and delayed tumor growth (Figure S1B). Beneficial effect of FL deficiency is also observed with sunitinib, an inhibitor of the FL-signaling pathway[91] (Figure S1C). High and low FL levels are also associated with delayed growth of YUMM1.7 melanoma (Figures 1E and S1G), an immunologically "cold" model derived from a tumor in $Braf^{V600E}Pten/Cdk2a^{-/-}$ mice.[92] In contrast, survival increased and tumor growth decreased along with FL levels in mice bearing subcutaneous MC38 colon carcinoma, a model of a "hot" tumor (Figures 1F and S1H). We speculated that the non-linear relationship between survival and FL levels in cold tumors is explained by FL effect on the homeostasis of DCs.

To define the short-/long-term consequences of FL loss and overexpression on DCs and other myeloid populations in tumor-bearing mice, we measured fold change (Figure 1C) and frequency (Figure S1E) of the relevant cell subsets in dLNs from the three groups of mice: WT_{B16}, $FL^{-/-}{}_{B16}$, and $WT_{B16\text{-}FL}$. In the context of tumor growth, the proportions of rDC1, rDC2, and pDCs in the dLNs show sustained positive relationship with FL levels (Figures 1C and S1E). In contrast, mDC1 and mDC2 display a transient increase. LC and infMo frequencies are increased in the $FL^{-/-}$ setting compared with controls. Resident monocyte, Mph, and monocyte-derived DC (moDC) frequencies display no correlation with FL levels at any time (Figures 1C and S1E). Thus, the experimental change in FL levels during tumor development is associated with changes in the proportion of cDCs in dLNs.

To evaluate functional phenotypes, we used t-SNE analysis of the flow cytometry data at day 5 (Figure 1D). The levels of expression of MHC class II, CD86, and CD40 on LCs, mDCs, and other DCs in the dLNs of FL-deficient mice (Figure 1D, left) remain on a par with control (Figure 1D, center) and FL-overexpressing mice (Figure 1D, right), as confirmed by their mean fluorescence intensity (MFI) (Figure S1F). Thus, in FL-dependent DC-deficient mice, the tumor-draining LNs still contain functional APCs. We conclude that FL is necessary for the recruitment of cDCs and pDCs to the tumor but that FL is dispensable for other APCs, which may initiate the effector T cell responses, as seen in non-tumor contexts[83,93] and in cancer.[94,95]

The absence of FL leads to decreased Treg and enhanced Teff response during tumor development

To understand how changes in DC populations in different FL contexts influence frequencies of Tregs and Teffs, we examined flow cytometric profiles of dLNs and established tumors in the three mouse cohorts. At day 11 of tumor growth, $FL^{-/-}{}_{B16}$ mice experience a marked decrease in frequency and number of Tregs in both organs compared with WT_{B16}, associated with an increase of Th frequency in dLNs and tumors and an increase of CTLs in tumors (Figures 2A and S2B). In $WT_{B16\text{-}FL}$ mice, Tregs are increased in both organs and CTLs are increased in tumors, but Th cells show opposite trends in the dLNs and in tumors compared with WT_{B16} (Figure 2A). Similar results were obtained in $WT^{+rFL}{}_{B16}$ mice (Figure 2B). Thus, FL loss or overexpression translates into changes in Treg and Teff frequencies.

To investigate the functional status of the Treg/Teff populations, we measured expression of activation/functional markers on day 11 in the three groups of mice. In tumor Tregs (Figure 2C), CD44, CTLA-4 (a molecule essential for their suppressive function[96]), and PD-1 (Figure S2C) expression are positively correlated with FL level (and cDC frequency). Expression of IL-10, an immunosuppressive cytokine, is lower on the Tregs from both FL groups compared with control (Figure 2C). ICOS, a costimulatory receptor implicated in Treg expansion[97,98] and production of IL-10,[97,99] is expressed by half of the Tregs in dLNs in control mice, and while $ICOS^+$ proportion is increased in both FL groups. However, ICOS MFI remains low in $FL^{-/-}{}_{B16}$ group but very high in the FL^{Hi} setting (Figure S2D).

In contrast, the activated and functional Th and CTLs in the tumor are increased in both FL^{Lo}/FL^{Hi} groups, compared with WT_{B16}. Expression of CD25 on Th and CTLs (Figure 2C) is higher in the $FL^{-/-}$ group. PD-1 on CTLs is increased 3-fold in both FL groups, and both groups display an increase in IFN-γ production or granzyme-B expression in Th and CTLs, respectively. Thus, despite inverse changes in Treg frequencies and activation

(D) Activated Treg and Th cells show, respectively, direct and inverse correlation to DC frequencies in tumor dLNs. Graphs show linear regression analysis of merged data from mice described in (A), plotting the logarithmized percentages of a given DC's subset vs. $CD44^{Hi}$ activated/memory Treg or Th cells. Pearson's coefficient of correlation (Pcc), associated p value, and regression curve slope (a) are shown.
(E) FL levels impact Treg division in tumor dLNs. Spleen and LN pooled $CD45.1^+$CFSE-labeled sorted Tregs from tumor-free mice were injected i.v. into CD45.2 tumor-free mice (WT, black), WT_{B16} (gray), $FL^{-/-}{}_{B16}$ (blue), and $WT^{+rFL}{}_{B16}$ (red) CD45.2 mice. CFSE dilution in $CD45.1^+$ Tregs was evaluated 10 days after adoptive transfer (triplicate). Numbers in the histograms indicate percentages of cells that had undergone more than five divisions. Scatterplots summarize the corresponding percentages of $CFSE^{-/lo}$Tregs. For subfigures (A–C, E), mean ± SEM are shown in all scatter plots, and data were compared by Student's t tests.
(F) Kaplan-Meyer plots show loss of beneficial effect of FL/cDC deficiency in the absence of $CD4^+$ and $CD8^+$ T cells and the effect of ICBT on $FL^{-/-}{}_{B16}$ mice. Mice were treated at day 4 of tumor growth by anti-CD4 and anti-CD8-depleting antibodies or at days 5–8 and 8–11 by a cocktail of anti-CTLA4/anti-PD1 antibodies. Log rank tests were performed to compare groups (n = 5 per group, representative of 2 experiments).
*p < 0.05, **p < 0.01, ***p < 0.001, ****p < 0.0001 for all the subfigures.

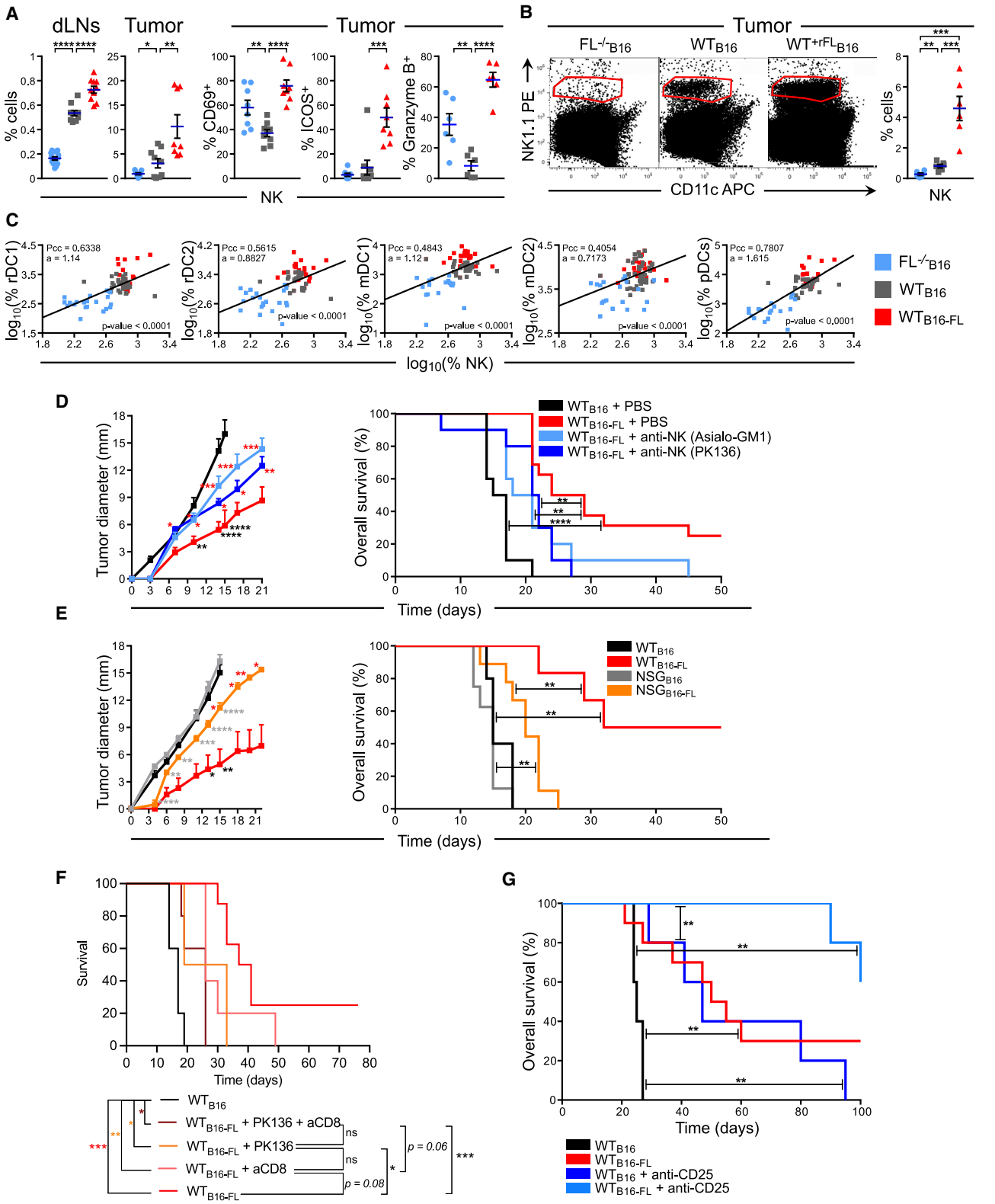

(legend on next page)

status, tumor-infiltrating Teffs in both FL loss and overexpression settings bear evidence of enhanced functionality.

As expected, the link between activated Tregs and FL levels is determined by FL-dependent DC levels. We detected highly significant and correlated relationship between DCs and activated Tregs in merged group analysis, but no or inverse correlation with activated Th (Figure 2D).

We confirmed that Treg changes are explained by their turnover, as observed in tumor-free mice.[83,100] We monitored fluorescence levels of CFSE-labeled CD45.1$^+$ Tregs in adoptively transferred tumor-bearing CD45.2 congenic mice with high/normal/absent FL and in tumor-free controls. 10 days later, Treg proliferation in dLNs was stimulated in the context of high FL, but no proliferation was detected in $FL^{-/-}{}_{B16}$ mice (Figure 2E).

Then, we determined whether the enhanced effector status observed in $FL^{-/-}$ mice is responsible for the improved survival in this group. We treated $FL^{-/-}{}_{B16}$ mice with depleting antibodies against CD4 and CD8. Treated $FL^{-/-}{}_{B16}$ mice display reduced overall survival (Figure 2F) and accelerated tumor growth (Figure S2E) compared with the untreated $FL^{-/-}{}_{B16}$ mice, similar to the WT_{B16} mice. Immune checkpoint blockade therapy (ICBT) in $FL^{-/-}{}_{B16}$ mice does not further improve survival, indicating that CTLA-4 and PD-1 ICs are already neutralized in this context.

Finally, DT-treated zDC^{DTR} BM chimeras, which, unlike the $FL^{-/-}$ mice, are only deficient in cDCs, but not in pDCs, present a 2-fold reduction in Treg, but not Th, proportion (Figure S2F), longer survival, and delayed tumor growth compared with PBS-treated chimeras (Figure S2G). Thus, lack of cDCs during tumor growth is sufficient to deplete Tregs and to improve survival.

Taken together, our results show that FL-dependent cDCs are necessary for the Treg-mediated tolerance induction in the tumor. cDC deficiency abrogates the Treg suppressive effect on CD4 and CD8 T cells and unleashes the adaptive anti-tumor immune response.

Excess of FL during tumor development stimulates recruitment and anti-tumor activity of NK cells

To determine the nature of the anti-tumor effect of FL overexpression, we evaluated the frequencies and activation of NK cells, important actors in the immune response against cancer,[72,101] in tumor-bearing mice. We found that NK cell frequencies are affected by variations of FL levels (Figures 3A and 3B). In $FL^{-/-}{}_{B16}$ mice, we observed a 3- to 5-fold reduction in the frequency and number of NK cells in dLN and tumors (Figures 3A and S3A). Conversely, in $WT_{B16\text{-}FL}$ group, we detected an increase in NK cell frequency (Figure 3A) and number (Figure S3A). We confirmed this in $WT^{+rFL}{}_{B16}$ mice (Figure 3B). We observed highly increased levels of CD69, ICOS, and granzyme-B on tumor-infiltrating NK cells in $WT_{B16\text{-}FL}$ mice compared with WT_{B16} (Figure 3A). Finally, correlation analyses revealed that NK cell frequencies in dLNs are positively related to pDC, rDC2, and rDC1 frequencies (Figure 3C). Of note, high levels of FL do not upregulate the FLT3 expression in NK cells and CTLs (Figure S3B). Thus, FL-mediated changes in DC frequencies translate into major changes in NK cell abundance and activity in tumor-bearing mice.

To test whether NK cells are necessary for the beneficial effect of FL overexpression, we used $WT_{B16\text{-}FL}$ mice depleted of NK cells using anti-NK mAbs. NK-depleted $WT_{B16\text{-}FL}$ mice display accelerated tumor growth and reduced overall survival compared with untreated mice (Figure 3D). Compared with the WT_{B16} group, NK-depleted $WT_{B16\text{-}FL}$ mice still fare slightly better, with delayed tumor growth and extended survival (Figure 3D). Thus, NK cell increase is necessary but not sufficient for the control of tumor growth by FL overexpression.

To address the role of the other immune cells, we used NSG mice, which, in addition to NK absence, also lack mature B and T cells and have defective myeloid cells. The beneficial effect of FL overexpression is abrogated in NSG mice (Figure 3E), reproducing the effect of NK depletion in immune-proficient C57Bl/6 mice. Thus, NK cells are the dominant subset responsible for the anti-tumor effect of FL overexpression. Of note, B16-FL tumors do not grow faster than B16 in NSG mice (Figure 3E) and have similar growth *in vitro,*[102] excluding a direct effect of FL on tumor proliferation.

As NK cells recruit CTLs during anti-tumor response,[103–105] and as we found more activated CTLs in B16-FL tumors (Figure 2C), we ablated CD8$^+$ T cells alone or together with NK1.1$^+$ cells with cell-depleting antibodies in B16-FL-bearing mice.

Figure 3. FL overexpression favors *in vivo* recruitment and anti-tumor activity of NK cells and synergizes with Treg depletion to improve mouse survival

(A) Left: scatterplots show the frequencies of NK1.1$^+$CD11c^{int} NK cells among live lymphocytes in dLN (n = 10–14 per group) or tumor (n = 8–9 per group) at day 11 post-inoculation for WT_{B16} (black), $FL^{-/-}{}_{B16}$ (blue), and $WT_{B16\text{-}FL}$ (red) groups (3 pooled experiments). Right: scatterplots depict the proportion of NK cells expressing CD69, ICOS (n = 8–9 per group), and granzyme-B (n = 6 per group) in the tumor for the same mice.

(B) Dot plots show the percentage of NK cells in the tumor at day 10 after inoculation. Scatterplots show corresponding NK cell mean frequency among lymphoid cells (n = 6 per group). Data shown and error bars in (A) and (B) are expressed as means ± SEM.

(C) NK cells show positive correlation to DC frequencies in tumor dLNs. Graphs show the linear regression analysis of merged data from mice described in (A), plotting as in Figure 2D. Pearson's coefficient of correlation (Pcc), associated p value, and regression curve slope (a) are shown.

(D) Graphs show tumor growth and overall survival of mice from the following groups: WT_{B16} (black, n = 10), $WT_{B16\text{-}FL}$ treated with two injections of PBS (red, n = 16) or NK-depleting mAbs (Asialo-GM1, light blue, n = 10; or PK136, dark blue, n = 10).

(E) Graphs show the tumor growth/overall survival of WT_{B16} (black, n = 5), $WT_{B16\text{-}FL}$ (red, n = 6), NSG_{B16} (gray, n = 8), and $NSG_{B16\text{-}FL}$ (orange, n = 9) mice.

(F) Overall survival of mice: control WT_{B16} (black, n = 5), untreated $WT_{B16\text{-}FL}$ (red, n = 8), or $WT_{B16\text{-}FL}$ treated with anti-NK-depleting mAbs (PK136, orange, n = 4), anti-CD8-depleting antibodies ($WT_{B16\text{-}FL}$ + anti-CD8, pink, n = 5), or both ($WT_{B16\text{-}FL}$ + anti-CD8 + PK136, maroon, n = 5). Survival curves were compared using log rank tests.

(G) Synergistic effect of FL overexpression and Treg depletion on survival of melanoma-bearing mice. Graph shows the overall survivals of WT_{B16} (black, n = 5), $WT^{+rFL}{}_{B16}$ (red, n = 10), WT_{B16} + anti-CD25-depleting mAb (dark blue, n = 5), and $WT^{+rFL}{}_{B16}$ + anti-CD25-depleting mAb (light blue, n = 5). All survival curves were compared using log rank tests, whereas tumor growth timepoints were individually compared (timepoint-matched) using Student's t tests. For the left graphs of (D and E), asterisks match the group color against which the comparison was made. *p < 0.05, **p < 0.01, ***p < 0.001, ****p < 0.0001.

Isolated depletion of $CD8^+$ cells compromises survival of $WT_{B16\text{-}FL}$ mice, but the effect did not reach statistical significance, while survival of $WT_{B16\text{-}FL}$ mice with isolated depletion of NK cells is significantly lower than the untreated $WT_{B16\text{-}FL}$ mice (Figures 3F and S3C). However, survival is further compromised in the absence of both $NK1.1^+$ cells and CTLs. We conclude that $CD8^+$ T cells contribute to the anti-tumor response led by NK cells in an FL^{Hi} context.

Synergistic effect of FL overexpression and Treg depletion or ICBT on tumor growth and mouse survival

To test whether FL overexpression and Treg depletion cooperate in anti-tumor activity, we injected B16- or B16-FL-bearing WT mice with Treg-depleting anti-CD25 mAb. The beneficial effects of isolated Treg depletion or FL treatment alone are similar, with 2-fold extension in survival compared with untreated mice (Figure 3G). The combination therapy further improves survival, with a majority of mice surviving over 100 days, five times over the untreated (Figures 3G and S3D). Treatment of $WT_{B16\text{-}FL}$ mice with CTLA-4, but not with PD-1, ICBT also cooperates with FL overexpression (Figures S3E and S3F). Thus, FL overexpression and Treg depletion/ICBT combination produce a synergistic effect against experimental tumors in mice.

The increase in $NK1.1^+$ cells by FL overexpression is mainly due to the recruitment of fully mature NK cells to the tumor

While most $NK1.1^+$ cells are bona fide NK cells ($EOMES^+CD49a^-$), the $NK1.1^+$ population also contains an ILC1 subset ($EOMES^-CD49a^+$) and a sub-population of ILC3 ($EOMES^-ROR\gamma T^+$). Moreover, we wondered whether iNKT cells ($TCRV\alpha14J\alpha18^+CD3^+NK1.1^+$) are also modulated by FL overexpression. We thus analyzed $NK1.1^+$ subpopulations in B16/B16-FL tumors and dLNs to discriminate between these subsets. We confirmed that *bona fide* NK cells accumulate in the tumor and dLNs in B16-FL-bearing mice (Figures 4A—4C). FL also induces full maturation of NK cells in the B16-FL tumor, illustrated by increased CD11b and lower CD27 expression[106] compared with NK_{cells} from B16 tumors (Figure 4D). ILCs are less consistently affected by FL overexpression: ILC1 are increased in B16-FL tumors compared with control (Figure 4B) but not in the dLNs (Figure 4C). In contrast, ILC3 accumulate in dLN from B16-FL but not in the tumor (Figures 4B and 4C). The frequency of iNKT cells in the tumor and the dLNs is lower in the B16-FL group (Figures 4B and 4C), excluding a significant role for these cells in this context. Overall, ILCs represent a minority of the $NK1.1^+$ cells in tumors and dLNs of WT_{B16FL} mice (Figures 4B, 4C, and S4). We conclude that tumor-infiltrating NK cells are more mature in the presence of FL, while the FL effect on ILC subsets is heterogeneous.

cDCs control NK cell homeostasis *in vivo*

To determine whether the effect of FL on NK_{cells} is direct or indirect, we confirmed the absence of Flt3 receptor expression on mature NK cells (Figure 5A). Furthermore, NK progenitors from the BM do not express Flt3, contrary to CLPs (Figure 5B, top). Similar results were obtained for thymic-NK precursors (not shown). FL overexpression does not modify the frequencies (Figure 5C, bottom) and numbers (Figure S5A) of NK progenitors in the BM or in the thymus (not shown), consistent with *in vitro* data.[22] Taken together, these results exclude a direct role of FL in the accumulation of NK cells in dLNs and tumor sites.

To test whether the increase in NK cells in FL-overexpressing tumor-bearing mice is fostered by cDCs, we made a model that combines DC deficiency and FL overexpression: B16-FL tumor-bearing zDC^{DTR} BM chimeras, $zDC^{DTR}{}_{B16\text{-}FL}$. As expected, PBS-treated $zDC^{DTR}{}_{B16\text{-}FL}$ retain high cDC and NK frequencies, while DT-treated chimeras show a 40-fold reduction in the number of DCs but also an 8-fold decrease in NK cell proportions in the spleen/dLNs, despite B16-FL tumor presence (Figure 5C). This decrease in NK cells is not a result of an impaired NK cell differentiation in the BM (Figure S5B). Moreover, the cDC-mediated effect on NK cell levels is also observed in the absence of tumors (Figure 5C). This confirms that NK cell homeostasis *in vivo* is controlled by FL-dependent cDCs and not by FL overexpression directly.

To assess the contribution of the DC1 ($CD8^+$ rDCs and $CD103^+$ mDCs) subset in the control of NK cells homeostasis, we used the $Batf3^{-/-}$ BM chimera model of DC1 deficiency. Despite a two-thirds drop in DC1, these chimeras show modest NK depletion in comparison with the DT-treated zDC^{DTR} chimeras (Figure 5D compared with Figure 5C). Importantly, FL overexpression is no longer accompanied by NK cell increase (Figure 5D). We conclude that cDCs and especially DC1 are required for FL-associated increase in NK cells in tumor-bearing mice.

FL/dendritic cell paradox in cancer patients

We hypothesized that cancer patients expressing FL levels strongly deviating from the average may be similar to the experimental situations of FL loss and FL overexpression that we created in mice. Thus, we analyzed transcriptomic data from TCGA melanoma cancer (SKCM) project. We separated patient cases into three groups (low, medium, and high expression of *FL* mRNA) and examined putative links between *FL* levels and immune cell transcriptomic signatures in the tumor samples (see STAR Methods and Table S1). To estimate the abundance of DC1, DC2, pDC, Treg, and NK cell gene signatures, we calculated a "quantitative score" (QS) (see STAR Methods) representing the mean of expression of the genes composing each signature. Consistent with our observations in mice, QSs for all five immune cell subsets (DC1, DC2, pDC, NK, and Treg) are positively associated with *FL* expression levels (Figure 6A). DC1/DC2 gene signatures also strongly correlate with Treg and NK signature levels in these patients (Figure 6B), indicating conservation in humans of the biological relationship observed in mice. In addition, *FL,* but not a control gene (*DMD*), correlates with Treg and NK cell signature intensity (Figure 6C).

In mice, DCs may control NK cell homeostasis by IL-15 transpresentation to NK cells via IL-15 receptors (IL-15R) present at the DC surface.[28] Conversely, IL-2 can be produced by DCs[107] and favor NK proliferation.[108,109] To verify this in humans, we evaluated *IL15*, *IL15RA*, and *IL2* expression levels in relation to the expression of DC1, DC2, and NK signatures in the melanoma cancer patients. We show that *IL15* and *IL15RA* and, to a lesser extent, *IL2* expression are correlated to DC1, DC2, and NK cell signatures in these patients, suggesting that, in humans, DCs support NK cell peripheral homeostasis through IL-15

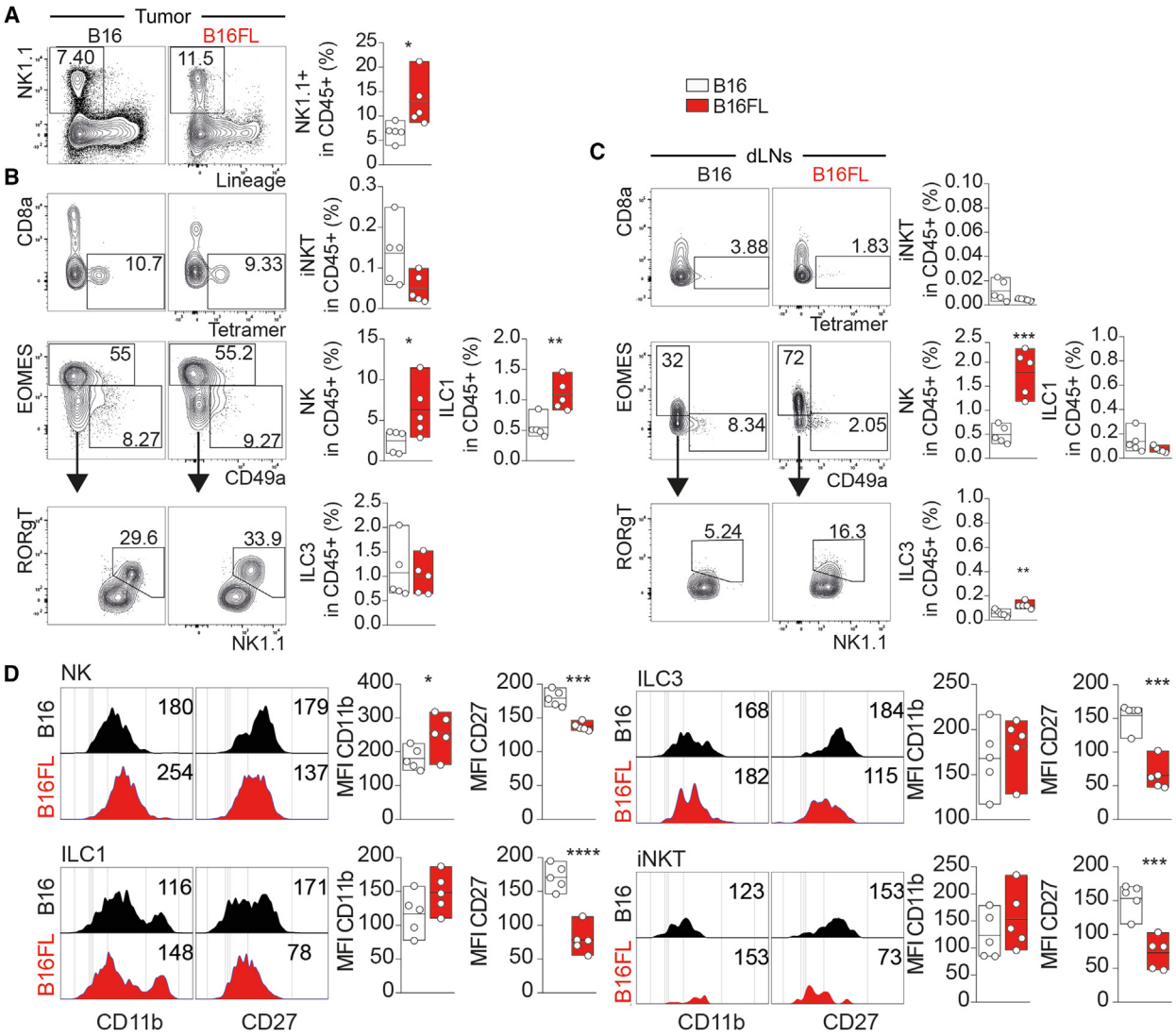

Figure 4. NK1.1^{+} cells recruited to tumors and dLNs in the FL^{Hi} setting are mainly fully mature NK cells

(A and B) Representative contour plots (left) and floating bar quantification plots (right) of the indicated cell subsets in tumors from $WT_{B16\text{-}FL}$ mice (red, n = 5) compared with WT_{B16} mice (white, n = 5). (A) Frequency of Lin^{-}(CD19^{-}F4/80^{-}Ly6G^{-}) NK1.1^{+} cells among live CD45^{+} cells.

(B and C) Frequency among tumor (B) or LN (C) CD45^{+}cells of: CD1d-Tetramer^{+}NK1.1^{+}CD3^{+}CD8^{-} iNKT cells, CD3^{-}EOMES^{+}CD49a^{-} NK cells, CD3^{-}EOMES^{-}CD49a^{+} ILC1 cells, and CD3^{-}EOMES^{-}CD49a^{-}RORgT^{+} ILC3 cells.

(D) Representative histogram plots and floating bar quantification plots of MFI for CD11b and CD27 on the tumor-infiltrating NKs, ILC1, ILC3, and iNKT. Student's t test (*p < 0.05, **p < 0.01, ***p < 0.001).

trans-presentation (Figures 6D, 6E, and S6A). The link between IL-2, NK cells, and DCs is less clear, as IL-2 may also drive DC expansion.[110]

Next, we analyzed survival and transcriptomic data from all cancers of the TCGA and TARGET projects. Consistent with the animal data, the paradoxical survival pattern is observed in three cancer types, including acute myeloid leukemia (AML), Wilms tumor, and pancreatic cancer, collectively representing at least 4.6% of new cancer cases each year in the USA (Figure 6F, top left). In other types of cancer, high *FL* levels are associated with beneficial outcome in 17 cancer types including SKCM (Figure 6F, top center) or with detrimental effect in seven cancer types (Figure 6F, top right). Individual cancers are shown in Figure S6B. To test how the level of DC transcriptomic signatures in patient tumors impact patient survival, we used DC-specific gene signatures and observed similar paradoxical, beneficial, or detrimental effect of DC signatures on survival, varying according to the DC subtype (DC1, DC2, or pDCs) and cancer type (Figures 6F and S6C–S6E). This shows that, in 35 human cancers, survival is significantly modulated by DC infiltration within the tumor. We also observed positive correlation of the effect of *FL* mRNA expression with cell signature strength in patients of each pooled cohort shown in Figure 6F, thus independently

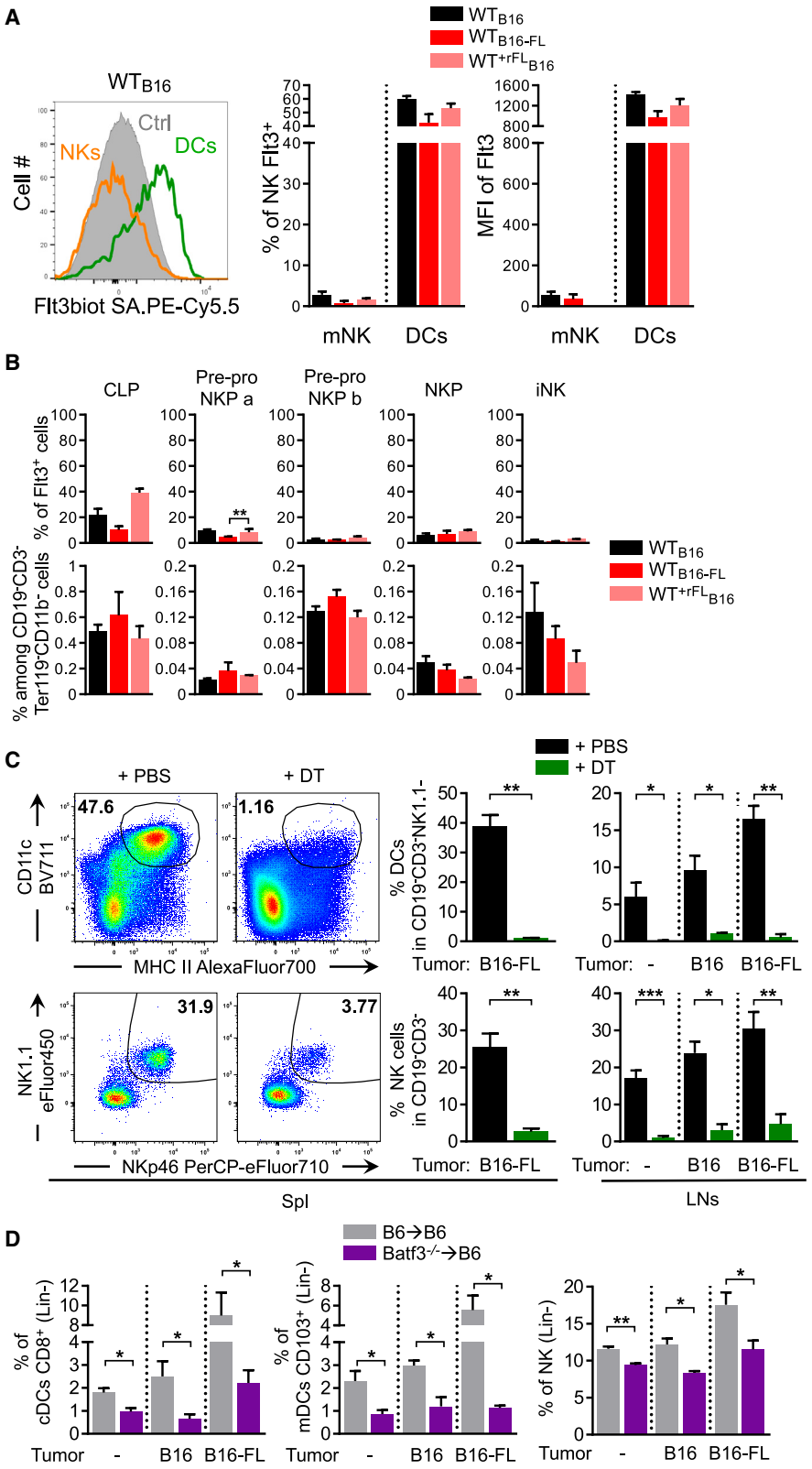

(legend on next page)

of the FL effect on survival (Figure 6G). Biological relationship between FL and immune cell infiltration is thus conserved between humans and mice.

Finally, we wondered whether high *FL* gene and low Treg signature expressions would synergize to improve survival in FL paradoxical cancers. In AML, WT, and PAAD cancers, the cohorts of patients with either low Treg signature abundance or high *FL* gene expression have better survival compared with other patients (Figures 6H and S6F). Impressively, patients with tumors showing combined high *FL* gene and low Treg signature survive significantly longer than other groups, with 70% of patients surviving longer than 5 years (Figure 6H), thus reproducing results we obtained in mice (Figure 3G).

DISCUSSION

Our study reveals that a tightly regulated level of FL is essential for tumor growth. We discovered paradoxical beneficial effect of high and low FL levels on anti-tumor immune response and that high *FL* and low Treg levels synergize to improve survival in mice and humans with certain cancers. We show that DC levels correlate to Treg and NK cell levels in both mice and humans, irrespective of the type of cancer, and provide genetic proof that cDCs govern NK cell, as well as Treg homeostasis in mice. In the cold tolerogenic B16 melanoma model, low levels of FL stimulate adaptive anti-tumor immune response, while high levels of FL favor innate anti-tumor immune response. Similar outcome is observed in the cold YUMM1.7 melanoma model. However, tumor growth and FL levels are negatively correlated in the hot MC38 colon carcinoma model. Our work thus reconciles and clarifies a body of conflicting reports on the beneficial/detrimental effect of FL on survival in cancer patients (see below).

We establish that FL effect on the immune response to melanoma tumors in mice is mediated through DCs. First, DCs are responsible for the recruitment of Tregs in the dLNs/tumor microenvironment. Then, Tregs keep in check the tumor-specific Teffs and NK cells and thus permit tumor growth.[70,72,78] This regulation is abrogated in FL-deficient mice, which lack cDCs and pDCs. Consequently, Teffs and their activation are increased, leading to an improved tumor control. This is consistent with multiple accounts of the central role of Teffs in tumor immune response.[71,111,112] $CD4^+$ Th cell levels are inversely correlated to FL-dependent DC levels, likely mediated by the FL-independent APCs in these mice. Teff recruitment/activation has been reported in tumor-free mice without DC[83,93] or with non-functional DCs[113] and in DC-deficient tumor-bearing mice,[114] reinforcing the idea that different APCs direct distinct T cell responses.[50]

We confirmed these results in sunitinib-treated mice and in the FL-independent zDC^{DTR} model of cDC depletion. This excludes putative compensation that may be at play in a constitutive knockout model. In the latter model, survival gain was more modest than in $FL^{-/-}$ mice, possibly explained by the absence of Th increase in the chimeras. In support, a 25% decrease in B16 growth in DT-treated zDC^{DTR} mice is reported by the Boyman group[110] (Figure 6H of their article). Also, zDC^{DTR} mice only lack cDCs, while $FL^{-/-}$ mice lack pDCs, cDCs, and, surprisingly, moDCs, possibly an indirect consequence of the depletion of cDC/pDC. We did not observe any clinical difference in DT-treated vs. untreated $CD11c^{DTR}$ B16-bearing mice (not shown, corroborated by Raeber et al.[110]), probably because CD11c is also expressed on NK cells.[115,116] The evidence that both cDCs and pDCs may establish immune tolerance in cancer as in autoimmune disease is in agreement with the most recent literature.[58,94,117,118] Finally, depletion of $CD4^+$ and $CD8^+$ T cells abrogates the survival benefit in the $FL^{-/-}{}_{B16}$ mice, formally tying up tumor control in the FL^{Lo} setting to adaptive immune mechanisms.

In B16-bearing mice with high levels of FL, an increase in FL-dependent DCs favors recruitment of efficacious granzyme-B^+ NK cells. FL overexpression not only slows tumor growth but also results in complete tumor regression in a substantial proportion of mice. FL treatment was previously shown to boost NK cell numbers,[119] although this was considered a transient effect, insufficient for anti-tumor immune memory in some models.[120] Yet, in the highly tolerogenic B16 model, combination therapies with FL produced remarkable results.[20,44] We formally show that the beneficial effect of FL on survival is abolished by NK cell ablation to an extent similar to that seen in immunodeficient mice. Noteworthily, NK cell depletion alone does not accelerate B16 tumor growth (Figures S3G and S3H; Wilson and coworkers[121,122]). In agreement with Salmon et al.,[44] we also observe an increase in activated CTLs in the tumors of FL-treated mice. This increase may be explained by the direct recruitment of $CD8^+$ T cells to the tumor by $CD103^+$ DC1 cells, as proposed by these authors, or by "help" from NK cells.[103–105,123] These mechanisms are not mutually exclusive. In any case, depletion of $CD8^+$ T cells further reduces survival of NK-depleted B16-FL-bearing mice, but isolated CD8 depletion has a weak effect, suggesting that both NK cells and CTLs are necessary for the anti-tumor benefit of FL, but only the NK cells are sufficient to substantially improve survival.

Figure 5. cDCs control the homeostasis of NK cells

(A) Representative histogram (left) shows FLT3 expression in DCs (green) and NK cells (orange). DCs labeled with control antibody are in gray. Bar plots show the percentage of $Flt3^+$ cells and Flt3 MFI in the indicated populations from the dLNs of WT_{B16} mice at day 11 of tumor growth (n = 3 per group, representative of 2 experiments).

(B) NK precursor frequency and Flt3 expression in the BM of tumor-bearing mice. Bar plots show percentages of $Flt3^+$ NK precursors (top row) and percentages of NK precursors among live Lin^- cells ($CD19^-CD3^-Ter119^-CD11b^-$) (bottom row) in the BM from the indicated groups on day 11 (n = 3–6 per group).

(C) cDCs control NK cell homeostasis in the context of FL overexpression. Representative pseudo-color plots and bar quantification plots of DC and NK cell abundance in spleens and dLNs from $Zbtb46^{DTR} \rightarrow$ B6 BM chimeras mice treated for 11 days with PBS or DT and with or without B16 or B16-FL tumors (n = 3–6 per group, 2 experiments pooled).

(D) dLNs from B16 or B16-FL tumor-bearing or tumor-free chimeras reconstituted with BM cells from $Batf3^{-/-}$ mice show reduced proportions of rDC1 (left), mDC1 (center), and NK_{cells} (right) at day 11 post-inoculation compared with non-chimera controls (n = 3 per group).

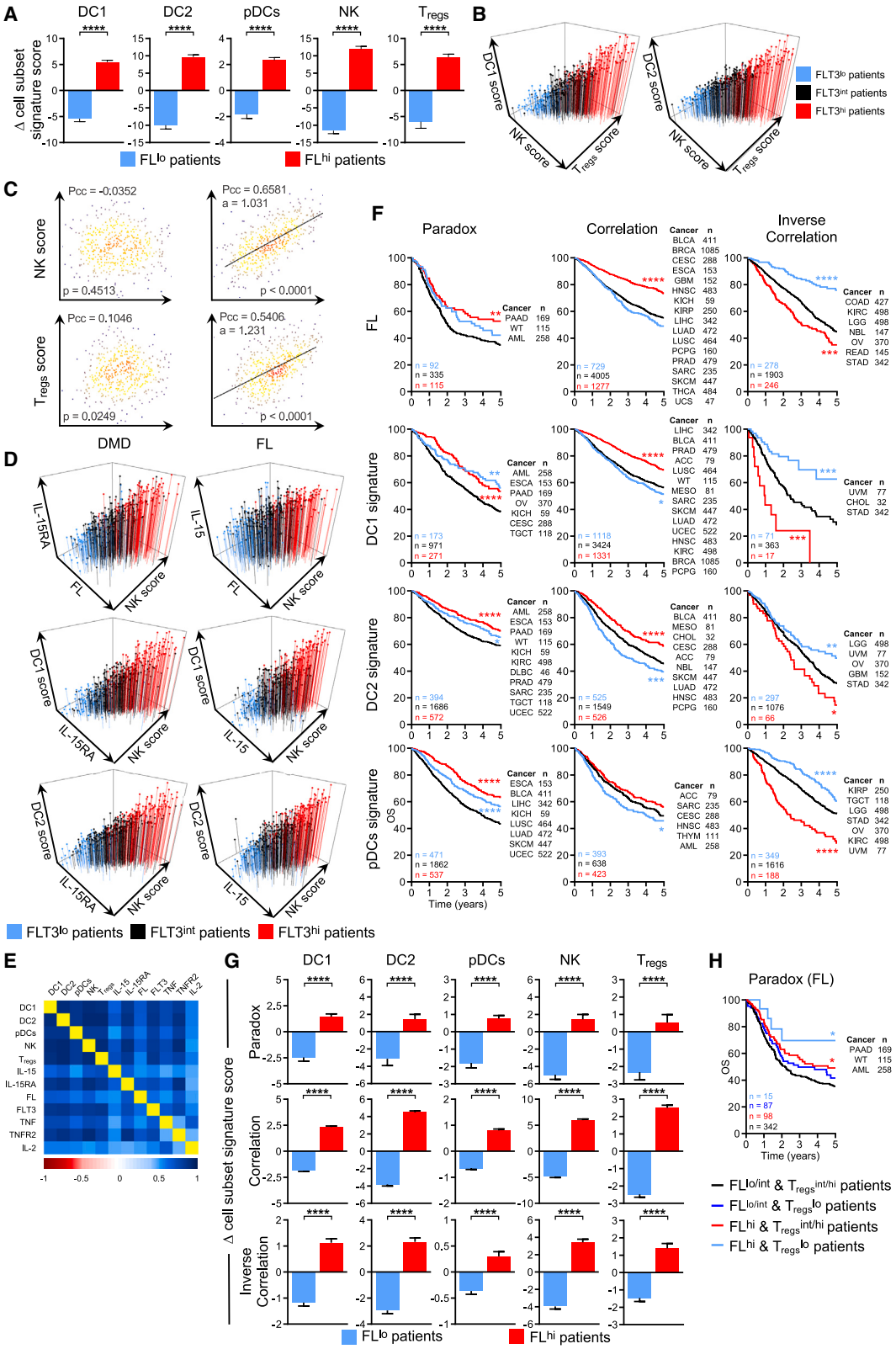

(legend on next page)

Also, we provide genetic proof that NK cell homeostasis is maintained by FL-dependent zDC$^+$ cDCs, as their depletion induces profound NK cell deficiency despite the high levels of FL. Absence of changes in NK precursors in the BM also argues against a direct FL effect on NK cell differentiation despite evidence that FL spreads to the BM.[2,89] Noticeably, only DCs express the FLT3 receptor in the tumor environment.[124] High levels of FL do not modulate FLT3 expression in NK$_{cells}$ and CD8$^+$ T$_{cells}$ contrary to DC.[125,126] Experiments in a DC1-less *Batf3*$^{-/-}$chimera model, with 70% drop in DC1 and 30% decrease in NK cells, suggest that DC1 subset is at least partially responsible for NK cell number maintenance. While we cannot exclude that the remaining DC1 are sufficient to maintain NK numbers in this model, it is likely that other FL-dependent DC subsets are necessary for NK cell homeostasis.

Human cancer patient data show a clear positive correlation between FL levels and DC/NK cell and *IL15/IL15RA* expression. This argues that DC control of NK cells is mediated by IL-15/IL-15R in humans, a mechanism determined by a wealth of studies in mice[28,29,30,32,33] and also reported to stimulate CTLs.[127]

Our results highlight that the canonical "ménage à trois" between DCs, Tregs, and Teffs used to explain immune regulation[128] is actually a "foursome" that includes NK cells (graphical abstract and supplemental discussion). Supporting this view is recent evidence that NK cells help recruit DCs in the tumor by producing chemokines[35] or FL[34] themselves. The refined view on this multiplayer equilibrium may help to identify promising therapeutic combinations to be targeted for tumor elimination. Our study also offers a solution to a problem complicating therapeutic use of FL in cancer. We find that an unfortunate consequence of FL treatment is an increase in activated Tregs in the dLNs and the tumor microenvironment, as in tumor-free mice.[83] Others found that pDCs, too, are able to promote suppressive capacities (IL-10 production) of Tregs through the ICOS/ICOSL pathway.[59,129–131] In our study, the numbers of ICOS$^+$ Tregs are correlated with FL and pDC levels. However, IL-10-expressing Tregs are at the highest level in the FL-normal setting, which may explain the very poor anti-tumor immune response at baseline FL levels. FL overexpression did not increase IL-10 production by tumor-infiltrating Tregs. Instead, they upregulate CTLA-4, another potent suppression mediator for Tregs. Therefore, to deliver the full therapeutic power of FL against cancer, it is essential to silence the FL effect on Tregs. Our results argue that a combination of FL treatment with Treg inhibition is a promising approach for anti-cancer treatment. Anti-CTLA-4 with or without anti-PD-1 ICBT also synergizes with FL excess but is ineffective in the FL-deficient context. Thus, CTLA-4 ICBT is more efficient in the Treg^{Hi} than in the Treg^{Lo} context, hinting that, in this model, Tregs and not Teffs are the main target of CTLA-4 ICBT. As a cautionary note, PD-1 ICBT activates and stimulates division of PD-1$^+$ Treg, leading to hyperprogressive disease in gastric cancer.[79] This may explain the disappointing outcome with this ICBT in the FL^{Hi} context (Figures S3E and S3F). Treg profiling may be necessary for selecting patients who will benefit from the FL/ICBT combination therapy.

Our analysis of human gene expression data shows, once again, that in cancer "*rien n'est tout noir*, *rien n'est tout blanc*": exceptionally high or low levels of *FL* expression have paradoxical beneficial effects in some cancers, an unexpected clinical outcome, and clear beneficial or detrimental effect in others. Similar results were obtained for DC1, DC2, and pDC transcriptomic signature expression, illustrating the pivotal role of DC in both rejection[43,44,132–134] and tolerance[40,58,94,114,135] of cancer. Importantly, our experimental results explain the mechanistic underpinnings of this heterogeneity, raising hopes that *FL* expression/DC characterization in diagnostic samples may help to predict treatment outcomes and determine patients who may benefit from immunotherapies aimed at boosting or inhibiting DCs. Indeed, the pleiotropic effects of FL that we have discovered in human gene expression data are reflected in mixed reports coming from FL clinical trials, some showing beneficial,[136–138] weak/null,[89,139,140] or detrimental effects for

Figure 6. The Flt3-L paradox in human cancers

(A) cDC, NK cell, and Treg gene expression signature levels correlate to FL expression levels independently of the survival profile in primary/metastatic SKCM cases. Histogram bars show the percentages of variation of the quantitative scores (QSs) of FL^{Lo} FL^{Hi} groups of patients relative to the QS of the group of patients with medium expression of *FL* mRNA (n = 447 patients).

(B) cDC, NK cell, and Treg gene signature QSs correlate together in melanoma cancer patients. 3D graphs show the variations of the indicated parameters for each patient from the SKCM cohort. Each dot represents one patient and is colored according to the associated *FLT3* gene expression: *FLT3* low (blue), intermediate (black), and high (red).

(C) 2D graphs illustrate the correlation between NK cell signature QS and *FL* or *DMD* (control) genes transcriptomic expression in each patient with melanoma. Plotting as in Figure 2D.

(D) *IL15* and *IL15RA* transcriptomic expression correlates with *FL* and *FLT3* expression and with NK cell signature QS in melanoma patients. 3D graphs show the variations of the indicated parameters for each patient from the SKCM cohort. *FLT3*^{lo} (blue), *FLT3*^{int} (black), and *FLT3*^{hi} (red) patient groups are depicted.

(E) Correlation heatmap of the indicated cell population QSs and the indicated gene expression in the melanoma patient cohort. Mean Pcc of *IL15RA* vs. others >0.74, mean Pcc of *IL15* vs. others >0.58, and mean Pcc of *IL2* vs. others >0.53. All correlations presented are significant ($p < 0.05$) with Pcc > 0.

(F) FL gene and DC gene signature expression have paradoxical effects on patient overall survival in some cancers and are beneficial or detrimental in others. Kaplan-Meyer graphs summarize the overall survival of pooled patients (high expression, red; intermediate, black; low, blue) with cancers in which *FL* gene, or DC1, DC2, and pDC signature expression levels have a paradoxical, beneficial, or detrimental effect on survival. List of cancer types included, cohort size, and log rank tests p value summary comparing low or high group vs. medium group survivals are indicated.

(G) DC, NK cell, and Treg gene signature expression levels correlate to *FL* gene expression levels independently of the survival profile in various cancers. QSs for the indicated cell subset-specific gene signatures were calculated as in (A) for each of the patients of every group (*FL*-lo/int/hi) shown in (F). Histogram bars show for each signature the percentages of variation relative to the intermediate group. Student's t tests were used to compare groups.

(H) Kaplan-Meyer graphs show overall survival of the indicated patient groups from FL-paradox cancers (AML, WT, and PAAD). Patients were separated according to their *FL* gene/Treg signature expression. Cohort size and log rank tests p value summary are indicated. *$p < 0.05$, **$p < 0.01$, ***$p < 0.001$, and ****$p < 0.0001$.

patients.[141,142] It is thus important to take into account that cancer location/origin may pre-determine the immune microenvironment composition.[143]

In some human cancers, FL has a growth effect on tumor cells.[144,145] In AML, ITD mutation may render *FLT3* constitutively active and lead to uncontrolled leukemic blast proliferation.[146] However, not all AML cells possess this mutation[147,148] and/or respond to FL.[144] FL inhibition in AML was deemed successful in some studies[149] but had mixed performance in others.[146,150,151] This direct effect of FL on the tumor in some AML may explain why high *FLT3* expression has a negative effect on the survival of some patients. But the FL effect on the immune system may explain cases where high *FL* expression has a beneficial effect on survival, a clinically important implication. Of note, homozygous $FLT3^{ITD/ITD}$ mice with constant FL signaling develop leukocytosis and progressive splenomegaly,[152] suggesting that FL therapeutic use should be carefully designed.

In conclusion, we present a biological equation that reveals the fine balancing act played by FL on immune response and tolerance, and even on the cancer cells themselves. At the center of this equation lies the unique ability of DCs to influence the immune response to cancer via the control of Treg and NK cell homeostasis. This equation invites a refined view on a body of pre-clinical and clinical data investigating the utility of FL against cancer and offers a fresh paradigm for treatment schemes in oncology. A boost of cDCs by recombinant FL may be beneficial when combined with Treg depletion or with ICBT.[20,44,153] Accordingly, blockade of FL signaling using FL inhibitors may also give therapeutic effect, particularly if supplemented by putative NK-stimulating therapies. Such a personalized approach may help harness the power of FL as a master immune regulator. Our results and others[112,118] also reveal the central role of FL-dependent DCs in the anti-tumor immune response in humans and in mice. Illuminating both sides of the DC effect on cancer paves the way for rational design of anti-cancer immunotherapies.

Limitations of the study

Our study was not designed to identify an epistatic relationship between individual FL-dependent DC subsets. It is possible that some subsets are required to initiate the anti-tumor effect while others are required for its maintenance. Dissecting the role of individual subsets may help determine when and how DC1, DC2, and/or pDCs recruit Teffs, Tregs, and NK cells during the development of FL^{Hi} or FL^{Lo} tumors.

Our observations in FL-deficient mice indicate that some FL-independent cell subsets participate in anti-tumor immune response. However, we did not seek to identify the FL-independent APCs able to prime Teffs in the absence of cDCs or to determine whether these function only in isolation or in concert with FL-dependent immune subsets. Deciphering the mechanisms behind the difference in immune responses in B16 vs. MC38 in the FL^{Lo} setting also requires more investigation.

Our human data analysis favors IL-15 trans-presentation as a likely mechanism by which DCs recruit NK cells in FL^{Hi} context in agreement with other studies.[28,29–31] However, we did not formally interrogate the cytokine/chemokines crosstalk between DC and NK. In mice, profiling/depleting IL-15 or IL-2 on relevant subsets may help determine whether these cytokines increase because DC numbers increase or if there were other means for NK-dependent anti-tumor response in FL^{Hi} mice. In support of the former possibility, in FL-treated tumor-free mice, Guimond et al. report an increase of 4.5- and 2-fold in blood and spleen, respectively, of IL-15 mRNA, while it remained constant per individual DC.[33]

We used an original method to estimate cell subset presence in bulk transcriptomic profiles from patient biopsies. However, all methods to detect cell abundance in bulk transcriptome data have their limits, and transcriptomic signatures for individual cell subsets remain imperfect. It may be useful in the future to characterize tumor-infiltrating DCs, Treg, and NK cells in cancer patients by other methods on a large scale.

STAR★METHODS

Detailed methods are provided in the online version of this paper and include the following:

- KEY RESOURCES TABLE
- RESOURCE AVAILABILITY
  - Lead contact
  - Materials availability
  - Data and code availability
- EXPERIMENTAL MODELS AND SUBJECT DETAILS
  - Mice
  - Cell lines
  - Subjects
- METHOD DETAILS
  - *In vivo* mouse tumor models
  - Treatments
  - Cells preparation
  - Immune cells phenotyping and flow cytometry analysis
  - Bioinformatic analysis of cancer patient data
- QUANTIFICATION AND STATISTICAL ANALYSIS

SUPPLEMENTAL INFORMATION

Supplemental information can be found online at https://doi.org/10.1016/j.xcrm.2023.101256.

ACKNOWLEDGMENTS

We thank Michel Nussenzweig and Paulo Vieira for $FL^{-/-}$ mice and discussions; Francois-Xavier Mauvais for $Batf3^{-/-}$ BM cells; Michel Nussenzweig for B16-FL tumor and rFL; Olivier Lantz for tumor cell lines; Jérome Mégret and Klara Velinzon for cell sorting; Damien Chaussabel, Maria Leite de Moraes, and Zoran Jankovic for help and advice; and Thomas Eisenreich, Kai-hui Yao, Fabrice Valette, Kim Nguyen, Christelle Enond, and Olivier Bregerie for technical help. The human results reported here exclusively used data generated by the TCGA/TARGET Research Networks: https://www.cancer.gov/ccg/research/genome-sequencing. P.R. and X.L. were supported by La Ligue Contre le Cancer (TANC16319) and China Scholarship Council (CSC202206240034) fellowships, respectively. This work was supported by INSERM, Université Paris Cité, La Fondation ARC (PJA20141201668) and the Institut National Du Cancer (PLBIO2019-075).

AUTHOR CONTRIBUTIONS

G.D.-J. conceived the study. G.D.-J., K.P., P.R., and P.G. designed the experiments. P.R., M.V., G.D.-J., X.L., E.P., and A.B. performed experiments and

analyzed the data. G.D.-J., P.R., K.P., and P.G. interpreted the data. P.G., B.M., and E.L.G. provided critical reagents, technical advice, and material support. P.R., M.V., and N.C. performed bioinformatic analysis. G.D.-J., K.P., and P.R. wrote the manuscript with input from all coauthors.

DECLARATION OF INTERESTS

The authors declare no competing interests.

Received: March 22, 2022
Revised: June 5, 2023
Accepted: October 2, 2023
Published: December 19, 2023

REFERENCES

1. Rosnet, O., Matteï, M.G., Marchetto, S., and Birnbaum, D. (1991). Isolation and chromosomal localization of a novel FMS-like tyrosine kinase gene. Genomics *9*, 380–385.
2. Waskow, C., Liu, K., Darrasse-Jèze, G., Guermonprez, P., Ginhoux, F., Merad, M., Shengelia, T., Yao, K., and Nussenzweig, M. (2008). The receptor tyrosine kinase Flt3 is required for dendritic cell development in peripheral lymphoid tissues. Nat. Immunol. *9*, 676–683. https://doi.org/10.1038/ni.1615.
3. Matthews, W., Jordan, C.T., Wiegand, G.W., Pardoll, D., and Lemischka, I.R. (1991). A receptor tyrosine kinase specific to hematopoietic stem and progenitor cell-enriched populations. Cell *65*, 1143–1152.
4. Lyman, S.D., James, L., Vanden Bos, T., de Vries, P., Brasel, K., Gliniak, B., Hollingsworth, L.T., Picha, K.S., McKenna, H.J., Splett, R.R., et al. (1993). Molecular cloning of a ligand for the flt3/flk-2 tyrosine kinase receptor: a proliferative factor for primitive hematopoietic cells. Cell *75*, 1157–1167. 0092-8674(93)90325-K [pii].
5. Lyman, S.D., James, L., Johnson, L., Brasel, K., de Vries, P., Escobar, S.S., Downey, H., Splett, R.R., Beckmann, M.P., and McKenna, H.J. (1994). Cloning of the human homologue of the murine flt3 ligand: a growth factor for early hematopoietic progenitor cells. Blood *83*, 2795–2801.
6. Christensen, J.L., and Weissman, I.L. (2001). Flk-2 is a marker in hematopoietic stem cell differentiation: a simple method to isolate long-term stem cells. Proc. Natl. Acad. Sci. USA *98*, 14541–14546. https://doi.org/10.1073/pnas.261562798.
7. D'Amico, A., and Wu, L. (2003). The early progenitors of mouse dendritic cells and plasmacytoid predendritic cells are within the bone marrow hemopoietic precursors expressing Flt3. J. Exp. Med. *198*, 293–303. https://doi.org/10.1084/jem.20030107.
8. McKenna, H.J., Stocking, K.L., Miller, R.E., Brasel, K., De Smedt, T., Maraskovsky, E., Maliszewski, C.R., Lynch, D.H., Smith, J., Pulendran, B., et al. (2000). Mice lacking flt3 ligand have deficient hematopoiesis affecting hematopoietic progenitor cells, dendritic cells, and natural killer cells. Blood *95*, 3489–3497.
9. Banchereau, J., and Steinman, R.M. (1998). Dendritic cells and the control of immunity. Nature *392*, 245–252.
10. Steinman, R.M. (2012). Decisions about dendritic cells: past, present, and future. Annu. Rev. Immunol. *30*, 1–22. https://doi.org/10.1146/annurev-immunol-100311-102839.
11. Fogg, D.K., Sibon, C., Miled, C., Jung, S., Aucouturier, P., Littman, D.R., Cumano, A., and Geissmann, F. (2006). A clonogenic bone marrow progenitor specific for macrophages and dendritic cells. Science *311*, 83–87. https://doi.org/10.1126/science.1117729.
12. Onai, N., Obata-Onai, A., Schmid, M.A., Ohteki, T., Jarrossay, D., and Manz, M.G. (2007). Identification of clonogenic common Flt3+M-CSFR+ plasmacytoid and conventional dendritic cell progenitors in mouse bone marrow. Nat. Immunol. *8*, 1207–1216. https://doi.org/10.1038/ni1518.
13. Naik, S.H., Sathe, P., Park, H.Y., Metcalf, D., Proietto, A.I., Dakic, A., Carotta, S., O'Keeffe, M., Bahlo, M., Papenfuss, A., et al. (2007). Development of plasmacytoid and conventional dendritic cell subtypes from single precursor cells derived in vitro and in vivo. Nat. Immunol. *8*, 1217–1226. https://doi.org/10.1038/ni1522.
14. Lee, J., Breton, G., Oliveira, T.Y.K., Zhou, Y.J., Aljoufi, A., Puhr, S., Cameron, M.J., Sékaly, R.P., Nussenzweig, M.C., and Liu, K. (2015). Restricted dendritic cell and monocyte progenitors in human cord blood and bone marrow. J. Exp. Med. *212*, 385–399. https://doi.org/10.1084/jem.20141442.
15. Liu, K., Victora, G.D., Schwickert, T.A., Guermonprez, P., Meredith, M.M., Yao, K., Chu, F.F., Randolph, G.J., Rudensky, A.Y., and Nussenzweig, M. (2009). In vivo analysis of dendritic cell development and homeostasis. Science *324*, 392–397. https://doi.org/10.1126/science.1170540.
16. Breton, G., Lee, J., Zhou, Y.J., Schreiber, J.J., Keler, T., Puhr, S., Anandasabapathy, N., Schlesinger, S., Caskey, M., Liu, K., and Nussenzweig, M.C. (2015). Circulating precursors of human CD1c+ and CD141+ dendritic cells. J. Exp. Med. *212*, 401–413. https://doi.org/10.1084/jem.20141441.
17. Dudziak, D., Kamphorst, A.O., Heidkamp, G.F., Buchholz, V.R., Trumpfheller, C., Yamazaki, S., Cheong, C., Liu, K., Lee, H.W., Park, C.G., et al. (2007). Differential antigen processing by dendritic cell subsets in vivo. Science *315*, 107–111. https://doi.org/10.1126/science.1136080.
18. Liu, K., Waskow, C., Liu, X., Yao, K., Hoh, J., and Nussenzweig, M. (2007). Origin of dendritic cells in peripheral lymphoid organs of mice. Nat. Immunol. *8*, 578–583. https://doi.org/10.1038/ni1462.
19. Anandasabapathy, N., Breton, G., Hurley, A., Caskey, M., Trumpfheller, C., Sarma, P., Pring, J., Pack, M., Buckley, N., Matei, I., et al. (2015). Efficacy and safety of CDX-301, recombinant human Flt3L, at expanding dendritic cells and hematopoietic stem cells in healthy human volunteers. Bone Marrow Transplant. *50*, 924–930. https://doi.org/10.1038/bmt.2015.74.
20. Curran, M.A., and Allison, J.P. (2009). Tumor vaccines expressing flt3 ligand synergize with ctla-4 blockade to reject preimplanted tumors. Cancer Res. *69*, 7747–7755. https://doi.org/10.1158/0008-5472.CAN-08-3289.
21. Zhang, Y., Fu, J., Shi, Y., Peng, S., Cai, Y., Zhan, X., Song, N., Liu, Y., Wang, Z., Yu, Y., et al. (2018). A new cancer immunotherapy via simultaneous DC-mobilization and DC-targeted IDO gene silencing using an immune-stimulatory nanosystem. Int. J. Cancer *143*, 2039–2052. https://doi.org/10.1002/ijc.31588.
22. Yu, H., Fehniger, T.A., Fuchshuber, P., Thiel, K.S., Vivier, E., Carson, W.E., and Caligiuri, M.A. (1998). Flt3 ligand promotes the generation of a distinct CD34(+) human natural killer cell progenitor that responds to interleukin-15. Blood *92*, 3647–3657.
23. Durai, V., Bagadia, P., Briseño, C.G., Theisen, D.J., Iwata, A., Davidson, J.T., 4th, Gargaro, M., Fremont, D.H., Murphy, T.L., and Murphy, K.M. (2018). Altered compensatory cytokine signaling underlies the discrepancy between Flt3(-/-) and Flt3l(-/-) mice. J. Exp. Med. *215*, 1417–1435. https://doi.org/10.1084/jem.20171784.
24. Kennedy, M.K., Glaccum, M., Brown, S.N., Butz, E.A., Viney, J.L., Embers, M., Matsuki, N., Charrier, K., Sedger, L., Willis, C.R., et al. (2000). Reversible defects in natural killer and memory CD8 T cell lineages in interleukin 15-deficient mice. J. Exp. Med. *191*, 771–780.
25. Cooper, M.A., Bush, J.E., Fehniger, T.A., VanDeusen, J.B., Waite, R.E., Liu, Y., Aguila, H.L., and Caligiuri, M.A. (2002). In vivo evidence for a dependence on interleukin 15 for survival of natural killer cells. Blood *100*, 3633–3638. https://doi.org/10.1182/blood-2001-12-0293.
26. Lodolce, J.P., Boone, D.L., Chai, S., Swain, R.E., Dassopoulos, T., Trettin, S., and Ma, A. (1998). IL-15 receptor maintains lymphoid homeostasis by supporting lymphocyte homing and proliferation. Immunity *9*, 669–676.

27. Fehniger, T.A., Suzuki, K., Ponnappan, A., VanDeusen, J.B., Cooper, M.A., Florea, S.M., Freud, A.G., Robinson, M.L., Durbin, J., and Caligiuri, M.A. (2001). Fatal leukemia in interleukin 15 transgenic mice follows early expansions in natural killer and memory phenotype CD8+ T cells. J. Exp. Med. *193*, 219–231.

28. Mortier, E., Woo, T., Advincula, R., Gozalo, S., and Ma, A. (2008). IL-15Rα chaperones IL-15 to stable dendritic cell membrane complexes that activate NK cells via trans presentation. J. Exp. Med. *205*, 1213–1225. https://doi.org/10.1084/jem.20071913.

29. Dubois, S., Mariner, J., Waldmann, T.A., and Tagaya, Y. (2002). IL-15Ralpha recycles and presents IL-15 In trans to neighboring cells. Immunity *17*, 537–547.

30. Burkett, P.R., Koka, R., Chien, M., Chai, S., Boone, D.L., and Ma, A. (2004). Coordinate expression and trans presentation of interleukin (IL)-15Ralpha and IL-15 supports natural killer cell and memory CD8+ T cell homeostasis. J. Exp. Med. *200*, 825–834. https://doi.org/10.1084/jem.20041389.

31. Sandau, M.M., Schluns, K.S., Lefrancois, L., and Jameson, S.C. (2004). Cutting edge: transpresentation of IL-15 by bone marrow-derived cells necessitates expression of IL-15 and IL-15R alpha by the same cells. J. Immunol. *173*, 6537–6541.

32. Hochweller, K., Striegler, J., Hämmerling, G.J., and Garbi, N. (2008). A novel CD11c.DTR transgenic mouse for depletion of dendritic cells reveals their requirement for homeostatic proliferation of natural killer cells. Eur. J. Immunol. *38*, 2776–2783. https://doi.org/10.1002/eji.200838659.

33. Guimond, M., Freud, A.G., Mao, H.C., Yu, J., Blaser, B.W., Leong, J.W., Vandeusen, J.B., Dorrance, A., Zhang, J., Mackall, C.L., and Caligiuri, M.A. (2010). In vivo role of Flt3 ligand and dendritic cells in NK cell homeostasis. J. Immunol. *184*, 2769–2775. https://doi.org/10.4049/jimmunol.0900685.

34. Barry, K.C., Hsu, J., Broz, M.L., Cueto, F.J., Binnewies, M., Combes, A.J., Nelson, A.E., Loo, K., Kumar, R., Rosenblum, M.D., et al. (2018). A natural killer-dendritic cell axis defines checkpoint therapy-responsive tumor microenvironments. Nat. Med. *24*, 1178–1191. https://doi.org/10.1038/s41591-018-0085-8.

35. Böttcher, J.P., Bonavita, E., Chakravarty, P., Blees, H., Cabeza-Cabrerizo, M., Sammicheli, S., Rogers, N.C., Sahai, E., Zelenay, S., and Reis e Sousa, C. (2018). NK Cells Stimulate Recruitment of cDC1 into the Tumor Microenvironment Promoting Cancer Immune Control. Cell *172*, 1022–1037.e14.e1014. https://doi.org/10.1016/j.cell.2018.01.004.

36. Brocker, T., Riedinger, M., and Karjalainen, K. (1997). Targeted expression of major histocompatibility complex (MHC) class II molecules demonstrates that dendritic cells can induce negative but not positive selection of thymocytes in vivo. J. Exp. Med. *185*, 541–550.

37. Steinman, R.M., and Nussenzweig, M.C. (2002). Avoiding horror autotoxicus: the importance of dendritic cells in peripheral T cell tolerance. Proc. Natl. Acad. Sci. USA *99*, 351–358. https://doi.org/10.1073/pnas.231606698.

38. Hawiger, D., Masilamani, R.F., Bettelli, E., Kuchroo, V.K., and Nussenzweig, M.C. (2004). Immunological unresponsiveness characterized by increased expression of CD5 on peripheral T cells induced by dendritic cells in vivo. Immunity *20*, 695–705.

39. Enk, A.H., Jonuleit, H., Saloga, J., and Knop, J. (1997). Dendritic cells as mediators of tumor-induced tolerance in metastatic melanoma. Int. J. Cancer *73*, 309–316.

40. Ghiringhelli, F., Puig, P.E., Roux, S., Parcellier, A., Schmitt, E., Solary, E., Kroemer, G., Martin, F., Chauffert, B., and Zitvogel, L. (2005). Tumor cells convert immature myeloid dendritic cells into TGF-beta-secreting cells inducing CD4+CD25+ regulatory T cell proliferation. J. Exp. Med. *202*, 919–929.

41. Sotomayor, E.M., Borrello, I., Rattis, F.M., Cuenca, A.G., Abrams, J., Staveley-O'Carroll, K., and Levitsky, H.I. (2001). Cross-presentation of tumor antigens by bone marrow-derived antigen-presenting cells is the dominant mechanism in the induction of T-cell tolerance during B-cell lymphoma progression. Blood *98*, 1070–1077.

42. Broz, M.L., Binnewies, M., Boldajipour, B., Nelson, A.E., Pollack, J.L., Erle, D.J., Barczak, A., Rosenblum, M.D., Daud, A., Barber, D.L., et al. (2014). Dissecting the tumor myeloid compartment reveals rare activating antigen-presenting cells critical for T cell immunity. Cancer Cell *26*, 638–652. https://doi.org/10.1016/j.ccell.2014.09.007.

43. Roberts, E.W., Broz, M.L., Binnewies, M., Headley, M.B., Nelson, A.E., Wolf, D.M., Kaisho, T., Bogunovic, D., Bhardwaj, N., and Krummel, M.F. (2016). Critical Role for CD103(+)/CD141(+) Dendritic Cells Bearing CCR7 for Tumor Antigen Trafficking and Priming of T Cell Immunity in Melanoma. Cancer Cell *30*, 324–336. https://doi.org/10.1016/j.ccell.2016.06.003.

44. Salmon, H., Idoyaga, J., Rahman, A., Leboeuf, M., Remark, R., Jordan, S., Casanova-Acebes, M., Khudoynazarova, M., Agudo, J., Tung, N., et al. (2016). Expansion and Activation of CD103(+) Dendritic Cell Progenitors at the Tumor Site Enhances Tumor Responses to Therapeutic PD-L1 and BRAF Inhibition. Immunity *44*, 924–938. https://doi.org/10.1016/j.immuni.2016.03.012.

45. Hubert, M., Gobbini, E., Couillault, C., Manh, T.P.V., Doffin, A.C., Berthet, J., Rodriguez, C., Ollion, V., Kielbassa, J., Sajous, C., et al. (2020). IFN-III is selectively produced by cDC1 and predicts good clinical outcome in breast cancer. Sci. Immunol. *5*, eaav3942. https://doi.org/10.1126/sciimmunol.aav3942.

46. Yamazaki, S., Dudziak, D., Heidkamp, G.F., Fiorese, C., Bonito, A.J., Inaba, K., Nussenzweig, M.C., and Steinman, R.M. (2008). CD8+ CD205+ splenic dendritic cells are specialized to induce Foxp3+ regulatory T cells. J. Immunol. *181*, 6923–6933.

47. Wang, L., Pino-Lagos, K., de Vries, V.C., Guleria, I., Sayegh, M.H., and Noelle, R.J. (2008). Programmed death 1 ligand signaling regulates the generation of adaptive Foxp3+CD4+ regulatory T cells. Proc. Natl. Acad. Sci. USA *105*, 9331–9336. https://doi.org/10.1073/pnas.0710441105.

48. del Rio, M.L., Bernhardt, G., Rodriguez-Barbosa, J.I., and Förster, R. (2010). Development and functional specialization of CD103+ dendritic cells. Immunol. Rev. *234*, 268–281. https://doi.org/10.1111/j.0105-2896.2009.00874.x.

49. Jones, A., Bourque, J., Kuehm, L., Opejin, A., Teague, R.M., Gross, C., and Hawiger, D. (2016). Immunomodulatory Functions of BTLA and HVEM Govern Induction of Extrathymic Regulatory T Cells and Tolerance by Dendritic Cells. Immunity *45*, 1066–1077. https://doi.org/10.1016/j.immuni.2016.10.008.

50. Yin, X., Chen, S., and Eisenbarth, S.C. (2021). Dendritic Cell Regulation of T Helper Cells. Annu. Rev. Immunol. *39*, 759–790. https://doi.org/10.1146/annurev-immunol-101819-025146.

51. Iberg, C.A., and Hawiger, D. (2020). Natural and Induced Tolerogenic Dendritic Cells. J. Immunol. *204*, 733–744. https://doi.org/10.4049/jimmunol.1901121.

52. Idoyaga, J., Fiorese, C., Zbytnuik, L., Lubkin, A., Miller, J., Malissen, B., Mucida, D., Merad, M., and Steinman, R.M. (2013). Specialized role of migratory dendritic cells in peripheral tolerance induction. J. Clin. Invest. *123*, 844–854. https://doi.org/10.1172/JCI65260.

53. Liu, V.C., Wong, L.Y., Jang, T., Shah, A.H., Park, I., Yang, X., Zhang, Q., Lonning, S., Teicher, B.A., and Lee, C. (2007). Tumor evasion of the immune system by converting CD4+CD25- T cells into CD4+CD25+ T regulatory cells: role of tumor-derived TGF-beta. J. Immunol. *178*, 2883–2892.

54. Zhou, G., and Levitsky, H.I. (2007). Natural regulatory T cells and de novo-induced regulatory T cells contribute independently to tumor-specific tolerance. J. Immunol. *178*, 2155–2162.

55. Norian, L.A., Rodriguez, P.C., O'Mara, L.A., Zabaleta, J., Ochoa, A.C., Cella, M., and Allen, P.M. (2009). Tumor-infiltrating regulatory dendritic cells inhibit CD8+ T cell function via L-arginine metabolism. Cancer Res. *69*, 3086–3094. https://doi.org/10.1158/0008-5472.CAN-08-2826.

56. Binnewies, M., Mujal, A.M., Pollack, J.L., Combes, A.J., Hardison, E.A., Barry, K.C., Tsui, J., Ruhland, M.K., Kersten, K., Abushawish, M.A., et al. (2019). Unleashing Type-2 Dendritic Cells to Drive Protective Antitumor CD4(+) T Cell Immunity. Cell *177*, 556–571.e16. https://doi.org/10.1016/j.cell.2019.02.005.

57. Laoui, D., Keirsse, J., Morias, Y., Van Overmeire, E., Geeraerts, X., Elkrim, Y., Kiss, M., Bolli, E., Lahmar, Q., Sichien, D., et al. (2016). The tumour microenvironment harbours ontogenically distinct dendritic cell populations with opposing effects on tumour immunity. Nat. Commun. *7*, 13720. https://doi.org/10.1038/ncomms13720.

58. Terra, M., Oberkampf, M., Fayolle, C., Rosenbaum, P., Guillerey, C., Dadaglio, G., and Leclerc, C. (2018). Tumor-Derived TGFbeta Alters the Ability of Plasmacytoid Dendritic Cells to Respond to Innate Immune Signaling. Cancer Res. *78*, 3014–3026. https://doi.org/10.1158/0008-5472.CAN-17-2719.

59. Conrad, C., Gregorio, J., Wang, Y.H., Ito, T., Meller, S., Hanabuchi, S., Anderson, S., Atkinson, N., Ramirez, P.T., Liu, Y.J., et al. (2012). Plasmacytoid dendritic cells promote immunosuppression in ovarian cancer via ICOS costimulation of Foxp3(+) T-regulatory cells. Cancer Res. *72*, 5240–5249. https://doi.org/10.1158/0008-5472.CAN-12-2271.

60. Faget, J., Bendriss-Vermare, N., Gobert, M., Durand, I., Olive, D., Biota, C., Bachelot, T., Treilleux, I., Goddard-Leon, S., Lavergne, E., et al. (2012). ICOS-ligand expression on plasmacytoid dendritic cells supports breast cancer progression by promoting the accumulation of immunosuppressive CD4+ T cells. Cancer Res. *72*, 6130–6141. https://doi.org/10.1158/0008-5472.CAN-12-2409.

61. Sisirak, V., Faget, J., Gobert, M., Goutagny, N., Vey, N., Treilleux, I., Renaudineau, S., Poyet, G., Labidi-Galy, S.I., Goddard-Leon, S., et al. (2012). Impaired IFN-α production by plasmacytoid dendritic cells favors regulatory T-cell expansion that may contribute to breast cancer progression. Cancer Res. *72*, 5188–5197. https://doi.org/10.1158/0008-5472.CAN-11-3468.

62. Faget, J., Sisirak, V., Blay, J.Y., Caux, C., Bendriss-Vermare, N., and Ménétrier-Caux, C. (2013). ICOS is associated with poor prognosis in breast cancer as it promotes the amplification of immunosuppressive CD4(+) T cells by plasmacytoid dendritic cells. OncoImmunology *2*, e23185. https://doi.org/10.4161/onci.23185.

63. Drobits, B., Holcmann, M., Amberg, N., Swiecki, M., Grundtner, R., Hammer, M., Colonna, M., and Sibilia, M. (2012). Imiquimod clears tumors in mice independent of adaptive immunity by converting pDCs into tumor-killing effector cells. J. Clin. Invest. *122*, 575–585. https://doi.org/10.1172/JCI61034.

64. Le Mercier, I., Poujol, D., Sanlaville, A., Sisirak, V., Gobert, M., Durand, I., Dubois, B., Treilleux, I., Marvel, J., Vlach, J., et al. (2013). Tumor promotion by intratumoral plasmacytoid dendritic cells is reversed by TLR7 ligand treatment. Cancer Res. *73*, 4629–4640. https://doi.org/10.1158/0008-5472.CAN-12-3058.

65. Liu, C., Lou, Y., Lizée, G., Qin, H., Liu, S., Rabinovich, B., Kim, G.J., Wang, Y.H., Ye, Y., Sikora, A.G., et al. (2008). Plasmacytoid dendritic cells induce NK cell-dependent, tumor antigen-specific T cell cross-priming and tumor regression in mice. J. Clin. Invest. *118*, 1165–1175. https://doi.org/10.1172/JCI33583.

66. Humbert, M., Guery, L., Brighouse, D., Lemeille, S., and Hugues, S. (2018). Intratumoral CpG-B promotes anti-tumoral neutrophil, cDC, and T cell cooperation without reprograming tolerogenic pDC. Cancer Res. *78*, 3280–3292. https://doi.org/10.1158/0008-5472.CAN-17-2549.

67. Wing, K., and Sakaguchi, S. (2010). Regulatory T cells exert checks and balances on self tolerance and autoimmunity. Nat. Immunol. *11*, 7–13. https://doi.org/10.1038/ni.1818.

68. Darrasse-Jèze, G., Bergot, A.S., Durgeau, A., Billiard, F., Salomon, B.L., Cohen, J.L., Bellier, B., Podsypanina, K., and Klatzmann, D. (2009). Tumor emergence is sensed by self-specific CD44hi memory Tregs that create a dominant tolerogenic environment for tumors in mice. J. Clin. Invest. *119*, 2648–2662. https://doi.org/10.1172/JCI36628.

69. Malchow, S., Leventhal, D.S., Nishi, S., Fischer, B.I., Shen, L., Paner, G.P., Amit, A.S., Kang, C., Geddes, J.E., Allison, J.P., et al. (2013). Aire-dependent thymic development of tumor-associated regulatory T cells. Science *339*, 1219–1224. https://doi.org/10.1126/science.1233913.

70. Darrasse-Jèze, G., and Podsypanina, K. (2013). How numbers, nature, and immune status of foxp3(+) regulatory T-cells shape the early immunological events in tumor development. Front. Immunol. *4*, 292. https://doi.org/10.3389/fimmu.2013.00292.

71. Chaput, N., Darrasse-Jèze, G., Bergot, A.S., Cordier, C., Ngo-Abdalla, S., Klatzmann, D., and Azogui, O. (2007). Regulatory T cells prevent CD8 T cell maturation by inhibiting CD4 Th cells at tumor sites. J. Immunol. *179*, 4969–4978.

72. Shimizu, J., Yamazaki, S., and Sakaguchi, S. (1999). Induction of tumor immunity by removing CD25+CD4+ T cells: a common basis between tumor immunity and autoimmunity. J. Immunol. *163*, 5211–5218.

73. Curiel, T.J., Coukos, G., Zou, L., Alvarez, X., Cheng, P., Mottram, P., Evdemon-Hogan, M., Conejo-Garcia, J.R., Zhang, L., Burow, M., et al. (2004). Specific recruitment of regulatory T cells in ovarian carcinoma fosters immune privilege and predicts reduced survival. Nat. Med. *10*, 942–949.

74. Woo, E.Y., Chu, C.S., Goletz, T.J., Schlienger, K., Yeh, H., Coukos, G., Rubin, S.C., Kaiser, L.R., and June, C.H. (2001). Regulatory CD4(+) CD25(+) T cells in tumors from patients with early- stage non-small cell lung cancer and late-stage ovarian cancer. Cancer Res. *61*, 4766–4772.

75. Liyanage, U.K., Moore, T.T., Joo, H.G., Tanaka, Y., Herrmann, V., Doherty, G., Drebin, J.A., Strasberg, S.M., Eberlein, T.J., Goedegebuure, P.S., and Linehan, D.C. (2002). Prevalence of regulatory T cells is increased in peripheral blood and tumor microenvironment of patients with pancreas or breast adenocarcinoma. J. Immunol. *169*, 2756–2761.

76. Wolf, A.M., Wolf, D., Steurer, M., Gastl, G., Gunsilius, E., and Grubeck-Loebenstein, B. (2003). Increase of regulatory T cells in the peripheral blood of cancer patients. Clin. Cancer Res. *9*, 606–612.

77. Sasada, T., Kimura, M., Yoshida, Y., Kanai, M., and Takabayashi, A. (2003). CD4+CD25+ regulatory T cells in patients with gastrointestinal malignancies: possible involvement of regulatory T cells in disease progression. Cancer *98*, 1089–1099.

78. deLeeuw, R.J., Kost, S.E., Kakal, J.A., and Nelson, B.H. (2012). The prognostic value of FoxP3+ tumor-infiltrating lymphocytes in cancer: a critical review of the literature. Clin. Cancer Res. *18*, 3022–3029. https://doi.org/10.1158/1078-0432.CCR-11-3216.

79. Kamada, T., Togashi, Y., Tay, C., Ha, D., Sasaki, A., Nakamura, Y., Sato, E., Fukuoka, S., Tada, Y., Tanaka, A., et al. (2019). PD-1^{+} regulatory T cells amplified by PD-1 blockade promote hyperprogression of cancer. Proc. Natl. Acad. Sci. USA *116*, 9999–10008. https://doi.org/10.1073/pnas.1822001116.

80. Onizuka, S., Tawara, I., Shimizu, J., Sakaguchi, S., Fujita, T., and Nakayama, E. (1999). Tumor rejection by in vivo administration of anti-CD25 (interleukin-2 receptor alpha) monoclonal antibody. Cancer Res. *59*, 3128–3133.

81. Bos, P.D., Plitas, G., Rudra, D., Lee, S.Y., and Rudensky, A.Y. (2013). Transient regulatory T cell ablation deters oncogene-driven breast cancer and enhances radiotherapy. J. Exp. Med. *210*, 2435–2466. https://doi.org/10.1084/jem.20130762.

82. Arce Vargas, F., Furness, A.J.S., Solomon, I., Joshi, K., Mekkaoui, L., Lesko, M.H., Miranda Rota, E., Dahan, R., Georgiou, A., Sledzinska, A., et al. (2017). Fc-Optimized Anti-CD25 Depletes Tumor-Infiltrating Regulatory T Cells and Synergizes with PD-1 Blockade to Eradicate Established Tumors. Immunity *46*, 577–586. https://doi.org/10.1016/j.immuni.2017.03.013.

83. Darrasse-Jèze, G., Deroubaix, S., Mouquet, H., Victora, G.D., Eisenreich, T., Yao, K.H., Masilamani, R.F., Dustin, M.L., Rudensky, A., Liu, K., and Nussenzweig, M.C. (2009). Feedback control of regulatory T cell

homeostasis by dendritic cells in vivo. J. Exp. Med. *206*, 1853–1862. https://doi.org/10.1084/jem.20090746.

84. Bigley, V., Haniffa, M., Doulatov, S., Wang, X.N., Dickinson, R., McGovern, N., Jardine, L., Pagan, S., Dimmick, I., Chua, I., et al. (2011). The human syndrome of dendritic cell, monocyte, B and NK lymphoid deficiency. J Exp Med. jem, 20101459, [pii]. https://doi.org/10.1084/jem.20101459.

85. Collin, M., Bigley, V., Haniffa, M., and Hambleton, S. (2011). Human dendritic cell deficiency: the missing ID? Nat. Rev. Immunol. *11*, 575–583. https://doi.org/10.1038/nri3046.

86. Randolph, G.J., Angeli, V., and Swartz, M.A. (2005). Dendritic-cell trafficking to lymph nodes through lymphatic vessels. Nat. Rev. Immunol. *5*, 617–628. https://doi.org/10.1038/nri1670.

87. Fujita, T., Teramoto, K., Ozaki, Y., Hanaoka, J., Tezuka, N., Itoh, Y., Asai, T., Fujino, S., Kontani, K., and Ogasawara, K. (2009). Inhibition of transforming growth factor-beta-mediated immunosuppression in tumor-draining lymph nodes augments antitumor responses by various immunologic cell types. Cancer Res. *69*, 5142–5150. https://doi.org/10.1158/0008-5472.CAN-08-2499.

88. Nakahara, T., Oba, J., Shimomura, C., Kido-Nakahara, M., and Furue, M. (2016). Early Tumor-Infiltrating Dendritic Cells Change their Characteristics Drastically in Association with Murine Melanoma Progression. J. Invest. Dermatol. *136*, 146–153. https://doi.org/10.1038/JID.2015.359.

89. Mach, N., Gillessen, S., Wilson, S.B., Sheehan, C., Mihm, M., and Dranoff, G. (2000). Differences in dendritic cells stimulated in vivo by tumors engineered to secrete granulocyte-macrophage colony-stimulating factor or Flt3-ligand. Cancer Res. *60*, 3239–3246.

90. Maraskovsky, E., Brasel, K., Teepe, M., Roux, E.R., Lyman, S.D., Shortman, K., and McKenna, H.J. (1996). Dramatic increase in the numbers of functionally mature dendritic cells in Flt3 ligand-treated mice: multiple dendritic cell subpopulations identified. J. Exp. Med. *184*, 1953–1962.

91. O'Farrell, A.M., Abrams, T.J., Yuen, H.A., Ngai, T.J., Louie, S.G., Yee, K.W.H., Wong, L.M., Hong, W., Lee, L.B., Town, A., et al. (2003). SU11248 is a novel FLT3 tyrosine kinase inhibitor with potent activity in vitro and in vivo. Blood *101*, 3597–3605.

92. Meeth, K., Wang, J.X., Micevic, G., Damsky, W., and Bosenberg, M.W. (2016). The YUMM lines: a series of congenic mouse melanoma cell lines with defined genetic alterations. Pigment Cell Melanoma Res. *29*, 590–597. https://doi.org/10.1111/pcmr.12498.

93. Ohnmacht, C., Pullner, A., King, S.B.S., Drexler, I., Meier, S., Brocker, T., and Voehringer, D. (2009). Constitutive ablation of dendritic cells breaks self-tolerance of CD4 T cells and results in spontaneous fatal autoimmunity. J. Exp. Med. *206*, 549–559. https://doi.org/10.1084/jem.20082394.

94. Kenkel, J.A., Tseng, W.W., Davidson, M.G., Tolentino, L.L., Choi, O., Bhattacharya, N., Seeley, E.S., Winer, D.A., Reticker-Flynn, N.E., and Engleman, E.G. (2017). An Immunosuppressive Dendritic Cell Subset Accumulates at Secondary Sites and Promotes Metastasis in Pancreatic Cancer. Cancer Res. *77*, 4158–4170. https://doi.org/10.1158/0008-5472.CAN-16-2212.

95. Hotblack, A., Holler, A., Piapi, A., Ward, S., Stauss, H.J., and Bennett, C.L. (2018). Tumor-Resident Dendritic Cells and Macrophages Modulate the Accumulation of TCR-Engineered T Cells in Melanoma. Mol. Ther. *26*, 1471–1481. https://doi.org/10.1016/j.ymthe.2018.03.011.

96. Wing, K., Onishi, Y., Prieto-Martin, P., Yamaguchi, T., Miyara, M., Fehervari, Z., Nomura, T., and Sakaguchi, S. (2008). CTLA-4 control over Foxp3+ regulatory T cell function. Science *322*, 271–275, 322/5899/271 [pii]. https://doi.org/10.1126/science.1160062.

97. Ito, T., Hanabuchi, S., Wang, Y.H., Park, W.R., Arima, K., Bover, L., Qin, F.X.F., Gilliet, M., and Liu, Y.J. (2008). Two functional subsets of FOXP3+ regulatory T cells in human thymus and periphery. Immunity *28*, 870–880.

98. Burmeister, Y., Lischke, T., Dahler, A.C., Mages, H.W., Lam, K.P., Coyle, A.J., Kroczek, R.A., and Hutloff, A. (2008). ICOS controls the pool size of effector-memory and regulatory T cells. J. Immunol. *180*, 774–782.

99. Herman, A.E., Freeman, G.J., Mathis, D., and Benoist, C. (2004). CD4+CD25+ T regulatory cells dependent on ICOS promote regulation of effector cells in the prediabetic lesion. J. Exp. Med. *199*, 1479–1489. https://doi.org/10.1084/jem.20040179.

100. Swee, L.K., Bosco, N., Malissen, B., Ceredig, R., and Rolink, A. (2009). Expansion of peripheral naturally occurring T regulatory cells by Fms-like tyrosine kinase 3 ligand treatment. Blood *113*, 6277–6287. https://doi.org/10.1182/blood-2008-06-161026.

101. Haller, O., Hansson, M., Kiessling, R., and Wigzell, H. (1977). Role of non-conventional natural killer cells in resistance against syngeneic tumour cells in vivo. Nature *270*, 609–611.

102. Danciu, C., Falamas, A., Dehelean, C., Soica, C., Radeke, H., Barbu-Tudoran, L., Bojin, F., Pînzaru, S.C., and Munteanu, M.F. (2013). A characterization of four B16 murine melanoma cell sublines molecular fingerprint and proliferation behavior. Cancer Cell Int. *13*, 75. https://doi.org/10.1186/1475-2867-13-75.

103. Kurosawa, S., Harada, M., Matsuzaki, G., Shinomiya, Y., Terao, H., Kobayashi, N., and Nomoto, K. (1995). Early-appearing tumour-infiltrating natural killer cells play a crucial role in the generation of anti-tumour T lymphocytes. Immunology *85*, 338–346.

104. Mocikat, R., Braumüller, H., Gumy, A., Egeter, O., Ziegler, H., Reusch, U., Bubeck, A., Louis, J., Mailhammer, R., Riethmüller, G., et al. (2003). Natural killer cells activated by MHC class I(low) targets prime dendritic cells to induce protective CD8 T cell responses. Immunity *19*, 561–569. https://doi.org/10.1016/s1074-7613(03)00264-4.

105. Fan, Z., Yu, P., Wang, Y., Wang, Y., Fu, M.L., Liu, W., Sun, Y., and Fu, Y.X. (2006). NK-cell activation by LIGHT triggers tumor-specific CD8+ T-cell immunity to reject established tumors. Blood *107*, 1342–1351. https://doi.org/10.1182/blood-2005-08-3485.

106. Chiossone, L., Chaix, J., Fuseri, N., Roth, C., Vivier, E., and Walzer, T. (2009). Maturation of mouse NK cells is a 4-stage developmental program. Blood *113*, 5488–5496. https://doi.org/10.1182/blood-2008-10-187179.

107. Zelante, T., Fric, J., Wong, A.Y.W., and Ricciardi-Castagnoli, P. (2012). Interleukin-2 production by dendritic cells and its immuno-regulatory functions. Front. Immunol. *3*, 161. https://doi.org/10.3389/fimmu.2012.00161.

108. Saadoun, D., Rosenzwajg, M., Joly, F., Six, A., Carrat, F., Thibault, V., Sene, D., Cacoub, P., and Klatzmann, D. (2011). Regulatory T-cell responses to low-dose interleukin-2 in HCV-induced vasculitis. N. Engl. J. Med. *365*, 2067–2077. https://doi.org/10.1056/NEJMoa1105143.

109. Gasteiger, G., Hemmers, S., Bos, P.D., Sun, J.C., and Rudensky, A.Y. (2013). IL-2-dependent adaptive control of NK cell homeostasis. J. Exp. Med. *210*, 1179–1187. https://doi.org/10.1084/jem.20122571.

110. Raeber, M.E., Rosalia, R.A., Schmid, D., Karakus, U., and Boyman, O. (2020). Interleukin-2 signals converge in a lymphoid-dendritic cell pathway that promotes anticancer immunity. Sci. Transl. Med. *12*, eaba5464. https://doi.org/10.1126/scitranslmed.aba5464.

111. Hung, K., Hayashi, R., Lafond-Walker, A., Lowenstein, C., Pardoll, D., and Levitsky, H. (1998). The central role of CD4(+) T cells in the antitumor immune response. J. Exp. Med. *188*, 2357–2368.

112. Cohen, M., Giladi, A., Barboy, O., Hamon, P., Li, B., Zada, M., Gurevich-Shapiro, A., Beccaria, C.G., David, E., Maier, B.B., et al. (2022). The interaction of $CD4^+$ helper T cells with dendritic cells shapes the tumor microenvironment and immune checkpoint blockade response. Nat. Can. (Ott.) *3*, 303–317. https://doi.org/10.1038/s43018-022-00338-5.

113. Kedmi, R., Najar, T.A., Mesa, K.R., Grayson, A., Kroehling, L., Hao, Y., Hao, S., Pokrovskii, M., Xu, M., Talbot, J., et al. (2022). A $ROR\gamma t^+$ cell instructs gut microbiota-specific T_{reg} cell differentiation. Nature *610*, 737–743. https://doi.org/10.1038/s41586-022-05089-y.

114. Diao, J., Gu, H., Tang, M., Zhao, J., and Cattral, M.S. (2018). Tumor Dendritic Cells (DCs) Derived from Precursors of Conventional DCs Are

Dispensable for Intratumor CTL Responses. J. Immunol. *201*, 1306–1314. https://doi.org/10.4049/jimmunol.1701514.

115. Laouar, Y., Sutterwala, F.S., Gorelik, L., and Flavell, R.A. (2005). Transforming growth factor-β controls T helper type 1 cell development through regulation of natural killer cell interferon-γ. Nat. Immunol. *6*, 600–607. https://doi.org/10.1038/ni1197.

116. Schleicher, U., Hesse, A., and Bogdan, C. (2005). Minute numbers of contaminant CD8+ T cells or CD11b+CD11c+ NK cells are the source of IFN-gamma in IL-12/IL-18-stimulated mouse macrophage populations. Blood *105*, 1319–1328. https://doi.org/10.1182/blood-2004-05-1749.

117. Yogev, N., Frommer, F., Lukas, D., Kautz-Neu, K., Karram, K., Ielo, D., von Stebut, E., Probst, H.C., van den Broek, M., Riethmacher, D., et al. (2012). Dendritic cells ameliorate autoimmunity in the CNS by controlling the homeostasis of PD-1 receptor(+) regulatory T cells. Immunity *37*, 264–275. https://doi.org/10.1016/j.immuni.2012.05.025.

118. Maier, B., Leader, A.M., Chen, S.T., Tung, N., Chang, C., LeBerichel, J., Chudnovskiy, A., Maskey, S., Walker, L., Finnigan, J.P., et al. (2020). A conserved dendritic-cell regulatory program limits antitumour immunity. Nature *580*, 257–262. https://doi.org/10.1038/s41586-020-2134-y.

119. Shaw, S.G., Maung, A.A., Steptoe, R.J., Thomson, A.W., and Vujanovic, N.L. (1998). Expansion of functional NK cells in multiple tissue compartments of mice treated with Flt3-ligand: implications for anti-cancer and anti-viral therapy. J. Immunol. *161*, 2817–2824.

120. Ciavarra, R.P., Somers, K.D., Brown, R.R., Glass, W.F., Consolvo, P.J., Wright, G.L., and Schellhammer, P.F. (2000). Flt3-ligand induces transient tumor regression in an ectopic treatment model of major histocompatibility complex-negative prostate cancer. Cancer Res. *60*, 2081–2084.

121. Wilson, K.A., Goding, S.R., Neely, H.R., Harris, K.M., and Antony, P.A. (2015). Depletion of $B220^{+}NK1.1^{+}$ cells enhances the rejection of established melanoma by tumor-specific $CD4^{+}$ T cells. OncoImmunology *4*, e1019196. https://doi.org/10.1080/2162402X.2015.1019196.

122. Park, S.H., Kyin, T., Bendelac, A., and Carnaud, C. (2003). The contribution of NKT cells, NK cells, and other gamma-chain-dependent non-T non-B cells to IL-12-mediated rejection of tumors. J. Immunol. *170*, 1197–1201. https://doi.org/10.4049/jimmunol.170.3.1197.

123. Martín-Fontecha, A., Thomsen, L.L., Brett, S., Gerard, C., Lipp, M., Lanzavecchia, A., and Sallusto, F. (2004). Induced recruitment of NK cells to lymph nodes provides IFN-gamma for T(H)1 priming. Nat. Immunol. *5*, 1260–1265. https://doi.org/10.1038/ni1138.

124. Garris, C.S., Arlauckas, S.P., Kohler, R.H., Trefny, M.P., Garren, S., Piot, C., Engblom, C., Pfirschke, C., Siwicki, M., Gungabeesoon, J., et al. (2018). Successful Anti-PD-1 Cancer Immunotherapy Requires T Cell-Dendritic Cell Crosstalk Involving the Cytokines IFN-gamma and IL-12. Immunity *49*, 1148–1161.e7. https://doi.org/10.1016/j.immuni.2018.09.024.

125. Cueto, F.J., and Sancho, D. (2021). The Flt3L/Flt3 Axis in Dendritic Cell Biology and Cancer Immunotherapy. Cancers *13*, 1525. https://doi.org/10.3390/cancers13071525.

126. Turner, A.M., Lin, N.L., Issarachai, S., Lyman, S.D., and Broudy, V.C. (1996). FLT3 receptor expression on the surface of normal and malignant human hematopoietic cells. Blood *88*, 3383–3390.

127. Di Pilato, M., Kfuri-Rubens, R., Pruessmann, J.N., Ozga, A.J., Messemaker, M., Cadilha, B.L., Sivakumar, R., Cianciaruso, C., Warner, R.D., Marangoni, F., et al. (2021). CXCR6 positions cytotoxic T cells to receive critical survival signals in the tumor microenvironment. Cell *184*, 4512–4530.e22. https://doi.org/10.1016/j.cell.2021.07.015.

128. Liu, Z., Gerner, M.Y., Van Panhuys, N., Levine, A.G., Rudensky, A.Y., and Germain, R.N. (2015). Immune homeostasis enforced by co-localized effector and regulatory T cells. Nature *528*, 225–230. https://doi.org/10.1038/nature16169.

129. Moseman, E.A., Liang, X., Dawson, A.J., Panoskaltsis-Mortari, A., Krieg, A.M., Liu, Y.J., Blazar, B.R., and Chen, W. (2004). Human plasmacytoid dendritic cells activated by CpG oligodeoxynucleotides induce the generation of CD4+CD25+ regulatory T cells. J. Immunol. *173*, 4433–4442.

130. Ito, T., Yang, M., Wang, Y.H., Lande, R., Gregorio, J., Perng, O.A., Qin, X.F., Liu, Y.J., and Gilliet, M. (2007). Plasmacytoid dendritic cells prime IL-10-producing T regulatory cells by inducible costimulator ligand. J. Exp. Med. *204*, 105–115.

131. Hanabuchi, S., Ito, T., Park, W.R., Watanabe, N., Shaw, J.L., Roman, E., Arima, K., Wang, Y.H., Voo, K.S., Cao, W., and Liu, Y.J. (2010). Thymic stromal lymphopoietin-activated plasmacytoid dendritic cells induce the generation of FOXP3+ regulatory T cells in human thymus. J. Immunol. *184*, 2999–3007. https://doi.org/10.4049/jimmunol.0804106.

132. Hildner, K., Edelson, B.T., Purtha, W.E., Diamond, M., Matsushita, H., Kohyama, M., Calderon, B., Schraml, B.U., Unanue, E.R., Diamond, M.S., et al. (2008). Batf3 deficiency reveals a critical role for CD8alpha+ dendritic cells in cytotoxic T cell immunity. Science *322*, 1097–1100. https://doi.org/10.1126/science.1164206.

133. Scarlett, U.K., Rutkowski, M.R., Rauwerdink, A.M., Fields, J., Escovar-Fadul, X., Baird, J., Cubillos-Ruiz, J.R., Jacobs, A.C., Gonzalez, J.L., Weaver, J., et al. (2012). Ovarian cancer progression is controlled by phenotypic changes in dendritic cells. J. Exp. Med. *209*, 495–506. https://doi.org/10.1084/jem.20111413.

134. Dixon, K.O., Tabaka, M., Schramm, M.A., Xiao, S., Tang, R., Dionne, D., Anderson, A.C., Rozenblatt-Rosen, O., Regev, A., and Kuchroo, V.K. (2021). TIM-3 restrains anti-tumour immunity by regulating inflammasome activation. Nature *595*, 101–106. https://doi.org/10.1038/s41586-021-03626-9.

135. Chaoul, N., Tang, A., Desrues, B., Oberkampf, M., Fayolle, C., Ladant, D., Sainz-Perez, A., and Leclerc, C. (2018). Lack of MHC class II molecules favors CD8(+) T-cell infiltration into tumors associated with an increased control of tumor growth. OncoImmunology *7*, e1404213. https://doi.org/10.1080/2162402X.2017.1404213.

136. Lynch, D.H., Andreasen, A., Maraskovsky, E., Whitmore, J., Miller, R.E., and Schuh, J.C. (1997). Flt3 ligand induces tumor regression and antitumor immune responses in vivo. Nat. Med. *3*, 625–631.

137. Esche, C., Subbotin, V.M., Maliszewski, C., Lotze, M.T., and Shurin, M.R. (1998). FLT3 ligand administration inhibits tumor growth in murine melanoma and lymphoma. Cancer Res. *58*, 380–383.

138. Wang, A., Braun, S.E., Sonpavde, G., and Cornetta, K. (2000). Antileukemic activity of Flt3 ligand in murine leukemia. Cancer Res. *60*, 1895–1900.

139. Disis, M.L., Rinn, K., Knutson, K.L., Davis, D., Caron, D., dela Rosa, C., and Schiffman, K. (2002). Flt3 ligand as a vaccine adjuvant in association with HER-2/neu peptide-based vaccines in patients with HER-2/neu-overexpressing cancers. Blood *99*, 2845–2850.

140. McNeel, D.G., Knutson, K.L., Schiffman, K., Davis, D.R., Caron, D., and Disis, M.L. (2003). Pilot study of an HLA-A2 peptide vaccine using flt3 ligand as a systemic vaccine adjuvant. J. Clin. Immunol. *23*, 62–72.

141. Miller, G., Pillarisetty, V.G., Shah, A.B., Lahrs, S., and DeMatteo, R.P. (2003). Murine Flt3 ligand expands distinct dendritic cells with both tolerogenic and immunogenic properties. J. Immunol. *170*, 3554–3564.

142. Solheim, J.C., Reber, A.J., Ashour, A.E., Robinson, S., Futakuchi, M., Kurz, S.G., Hood, K., Fields, R.R., Shafer, L.R., Cornell, D., et al. (2007). Spleen but not tumor infiltration by dendritic and T cells is increased by intravenous adenovirus-Flt3 ligand injection. Cancer Gene Ther. *14*, 364–371. https://doi.org/10.1038/sj.cgt.7701018.

143. Jiménez-Sánchez, A., Memon, D., Pourpe, S., Veeraraghavan, H., Li, Y., Vargas, H.A., Gill, M.B., Park, K.J., Zivanovic, O., Konner, J., et al. (2017). Heterogeneous Tumor-Immune Microenvironments among Differentially Growing Metastases in an Ovarian Cancer Patient. Cell *170*, 927–938.e20. https://doi.org/10.1016/j.cell.2017.07.025.

144. Serve, H., Flesch, K., Serve, S., Fenski, R., and Berdel, W.E. (1999). Expression and function of Flt3/flk2 in human tumor cell lines. Int. J. Oncol. *14*, 765–770.

145. Lisovsky, M., Estrov, Z., Zhang, X., Consoli, U., Sanchez-Williams, G., Snell, V., Munker, R., Goodacre, A., Savchenko, V., and Andreeff, M. (1996). Flt3 ligand stimulates proliferation and inhibits apoptosis of acute myeloid leukemia cells: regulation of Bcl-2 and Bax. Blood *88*, 3987–3997.

146. Fathi, A.T., and Chabner, B.A. (2011). FLT3 inhibition as therapy in acute myeloid leukemia: a record of trials and tribulations. Oncol. *16*, 1162–1174. https://doi.org/10.1634/theoncologist.2011-0084.

147. O'Farrell, A.M., Foran, J.M., Fiedler, W., Serve, H., Paquette, R.L., Cooper, M.A., Yuen, H.A., Louie, S.G., Kim, H., Nicholas, S., et al. (2003). An innovative phase I clinical study demonstrates inhibition of FLT3 phosphorylation by SU11248 in acute myeloid leukemia patients. Clin. Cancer Res. *9*, 5465–5476.

148. Meshinchi, S., Alonzo, T.A., Stirewalt, D.L., Zwaan, M., Zimmerman, M., Reinhardt, D., Kaspers, G.J.L., Heerema, N.A., Gerbing, R., Lange, B.J., and Radich, J.P. (2006). Clinical implications of FLT3 mutations in pediatric AML. Blood *108*, 3654–3661. https://doi.org/10.1182/blood-2006-03-009233.

149. Grunwald, M.R., and Levis, M.J. (2015). FLT3 Tyrosine Kinase Inhibition as a Paradigm for Targeted Drug Development in Acute Myeloid Leukemia. Semin. Hematol. *52*, 193–199. https://doi.org/10.1053/j.seminhematol.2015.03.004.

150. Chu, Y.H., Li, H., Tan, H.S., Koh, V., Lai, J., Phyo, W.M., Choudhury, Y., Kanesvaran, R., Chau, N.M., Toh, C.K., et al. (2015). Association of ABCB1 and FLT3 Polymorphisms with Toxicities and Survival in Asian Patients Receiving Sunitinib for Renal Cell Carcinoma. PLoS One *10*, e0134102. https://doi.org/10.1371/journal.pone.0134102.

151. Balaña, C., Gil, M.J., Perez, P., Reynes, G., Gallego, O., Ribalta, T., Capellades, J., Gonzalez, S., and Verger, E. (2014). Sunitinib administered prior to radiotherapy in patients with non-resectable glioblastoma: results of a phase II study. Targeted Oncol. *9*, 321–329. https://doi.org/10.1007/s11523-014-0305-1.

152. Lee, B.H., Tothova, Z., Levine, R.L., Anderson, K., Buza-Vidas, N., Cullen, D.E., McDowell, E.P., Adelsperger, J., Fröhling, S., Huntly, B.J.P., et al. (2007). FLT3 mutations confer enhanced proliferation and survival properties to multipotent progenitors in a murine model of chronic myelomonocytic leukemia. Cancer Cell *12*, 367–380. https://doi.org/10.1016/j.ccr.2007.08.031.

153. Curran, M.A., Montalvo, W., Yagita, H., and Allison, J.P. (2010). PD-1 and CTLA-4 combination blockade expands infiltrating T cells and reduces regulatory T and myeloid cells within B16 melanoma tumors. Proc. Natl. Acad. Sci. USA *107*, 4275–4280. https://doi.org/10.1073/pnas.0915174107.

154. Meredith, M.M., Liu, K., Darrasse-Jeze, G., Kamphorst, A.O., Schreiber, H.A., Guermonprez, P., Idoyaga, J., Cheong, C., Yao, K.H., Niec, R.E., and Nussenzweig, M.C. (2012). Expression of the zinc finger transcription factor zDC (Zbtb46, Btbd4) defines the classical dendritic cell lineage. J. Exp. Med. *209*, 1153–1165. https://doi.org/10.1084/jem.20112675.

155. Ivanov, I.I., Frutos, R.d.L., Manel, N., Yoshinaga, K., Rifkin, D.B., Sartor, R.B., Finlay, B.B., and Littman, D.R. (2008). Specific microbiota direct the differentiation of IL-17-producing T-helper cells in the mucosa of the small intestine. Cell Host Microbe *4*, 337–349, S1931-3128(08)00305-3 [pii]. https://doi.org/10.1016/j.chom.2008.09.009.

156. Villani, A.C., Satija, R., Reynolds, G., Sarkizova, S., Shekhar, K., Fletcher, J., Griesbeck, M., Butler, A., Zheng, S., Lazo, S., et al. (2017). Single-cell RNA-seq reveals new types of human blood dendritic cells, monocytes, and progenitors. Science *356*, eaah4573. https://doi.org/10.1126/science.aah4573.

157. Haniffa, M., Shin, A., Bigley, V., McGovern, N., Teo, P., See, P., Wasan, P.S., Wang, X.N., Malinarich, F., Malleret, B., et al. (2012). Human tissues contain CD141hi cross-presenting dendritic cells with functional homology to mouse CD103+ nonlymphoid dendritic cells. Immunity *37*, 60–73. https://doi.org/10.1016/j.immuni.2012.04.012.

158. McGovern, N., Shin, A., Low, G., Low, D., Duan, K., Yao, L.J., Msallam, R., Low, I., Shadan, N.B., Sumatoh, H.R., et al. (2017). Human fetal dendritic cells promote prenatal T-cell immune suppression through arginase-2. Nature *546*, 662–666. https://doi.org/10.1038/nature22795.

159. See, P., Dutertre, C.A., Chen, J., Günther, P., McGovern, N., Irac, S.E., Gunawan, M., Beyer, M., Händler, K., Duan, K., et al. (2017). Mapping the human DC lineage through the integration of high-dimensional techniques. Science *356*, eaag3009. https://doi.org/10.1126/science.aag3009.

160. Critchley-Thorne, R.J., Yan, N., Nacu, S., Weber, J., Holmes, S.P., and Lee, P.P. (2007). Down-regulation of the interferon signaling pathway in T lymphocytes from patients with metastatic melanoma. PLoS Med. *4*, e176. https://doi.org/10.1371/journal.pmed.0040176.

161. Novershtern, N., Subramanian, A., Lawton, L.N., Mak, R.H., Haining, W.N., McConkey, M.E., Habib, N., Yosef, N., Chang, C.Y., Shay, T., et al. (2011). Densely interconnected transcriptional circuits control cell states in human hematopoiesis. Cell *144*, 296–309. https://doi.org/10.1016/j.cell.2011.01.004.

162. Walter, G.J., Fleskens, V., Frederiksen, K.S., Rajasekhar, M., Menon, B., Gerwien, J.G., Evans, H.G., and Taams, L.S. (2016). Phenotypic, Functional, and Gene Expression Profiling of Peripheral CD45RA+ and CD45RO+ CD4+CD25+CD127(low) Treg Cells in Patients With Chronic Rheumatoid Arthritis. Arthritis Rheumatol. *68*, 103–116. https://doi.org/10.1002/art.39408.

163. Pesenacker, A.M., Wang, A.Y., Singh, A., Gillies, J., Kim, Y., Piccirillo, C.A., Nguyen, D., Haining, W.N., Tebbutt, S.J., Panagiotopoulos, C., and Levings, M.K. (2016). A Regulatory T-Cell Gene Signature Is a Specific and Sensitive Biomarker to Identify Children With New-Onset Type 1 Diabetes. Diabetes *65*, 1031–1039. https://doi.org/10.2337/db15-0572.

STAR★METHODS

KEY RESOURCES TABLE

REAGENT or RESOURCE	SOURCE	IDENTIFIER
Antibodies		
Anti-Asialo-GM1 (uncoupled, clone Poly21460)	BioLegend	Cat# 146002; RRID: AB_2562206
Anti-CD25 (uncoupled, clone 7D4)	BD Biosciences	Cat# 553072; RRID: AB_394604
Anti-CD3ε (clone 145-2C11)	BD Biosciences	Cat# 564379; RRID:AB_2738780
Anti CD3 (clone 17A2)	BioLegend	Cat# 100240; RRID: AB_2563427
Anti-CD4 (clone RM4-5)	BD Biosciences	Cat# 563050; RRID: AB_2737973
Anti-CD8α (clone 53–6.7)	BD Biosciences	Cat# 563152; RRID: AB_2738030
anti CD8α (clone 53–6.7)	BioLegend	Cat# 100747; RRID: AB_2563510
Anti-CD11b (clone M1/70)	eBioscience	Cat# 47-0112-82; RRID: AB_1603193
Anti CD11b (clone M1/70)	BioLegend	Cat# 101222; RRID: AB_493705
Anti-CD11c (clone HL3)	BD Biosciences	Cat# 563048; RRID: AB_2734778
anti CD11c (clone N418)	BioLegend	Cat# 117339; RRID: AB_2562414
Anti-CD16/32 (clone S17011E)	BioLegend	Cat# 156603; RRID: AB_2783137
Anti-CD19 (clone 6D5)	BioLegend	Cat# 115504; RRID: AB_313638
Anti-CD19 (clone 1D3)	BD Biosciences	Cat# 563235; RRID: AB_2738085
Anti-CD25 (clone 7D4)	BD Biosciences	Cat# 553072; RRID: AB_394604
Anti-CD27 (clone LG.7F9)	eBioscience	Cat# 11-0271-82; RRID: AB_465001
Anti-CD40 (clone HM40-3)	eBioscience	Cat# 11-0402-85; RRID: AB_465030
Anti-CD44 (clone IM7)	eBioscience	Cat# 35-0441-83; RRID: AB_469716
Anti-CD45 (clone 30-F11)	BD Biosciences	Cat# 564279; RRID: AB_2651134
Anti-CD49a (clone IM7)	BD Biosciences	Cat# 562113; RRID: AB_11153312
Anti-CD62L (clone MEL 14)	BioLegend	Cat# 104440; RRID: AB_2629685
Anti-CD69 (clone H1.2F3)	BD Biosciences	Cat# 553236; RRID: AB_394725
Anti-CD86 (clone GL1)	BD Biosciences	Cat# 564200; RRID: AB_2738665
Anti-CD103 (clone M290)	BD Biosciences	Cat# 564322; RRID: AB_2738744
Anti-CD135 (clone A2F10)	eBioscience	Cat# 13-1351-85; RRID: AB_466600
Anti CD135 (clone A2F10)	eBioscience	Cat# 15-1351-82; RRID: AB_494219
Anti-CD206 (clone C068C2)	BioLegend	Cat# 141720; RRID: AB_2562248
Anti-CTLA-4 (clone UC10-4F10-11)	BD Biosciences	Cat# 553720; RRID: AB_395005
Anti-DC-SIGN (clone MMD3)	eBioscience	Cat# 50-2094-82; RRID: AB_11219065
Anti-EOMES (clone X4-83)	BD Biosciences	Cat# 567166; RRID: AB_2916483
Anti-EpCAM (clone G8.8)	BD Biosciences	Cat# 563216; RRID: AB_2738075
anti-F4/80 (clone BM8)	BioLegend	Cat# 123105; RRID: AB_893499
Anti-F4/80 (clone BM8)	eBioscience	Cat# 15-4801-80; RRID: AB_468797
Anti-FoxP3 (clone FJK-16s)	eBioscience	Cat# 48-5773-82; RRID: AB_1518812
Anti-IFNγ (clone XMG1.2)	BD Biosciences	Cat# 554413; RRID: AB_398551
IgG2a, κ isotype Ctrl (MOPC-173)	BioLegend	Cat# 400201; RRID: AB_2927399
IgG2a kappa Isotype Control (eBR2a)	eBioscience	Cat# 15-4321-80; RRID: AB_657908
Anti-IL-2 (clone JES6-5H4)	BD Biosciences	Cat# 565186; RRID: AB_2739100
Anti-IL-10 (clone JSE5-16E3)	BD Biosciences	Cat# 554468; RRID: AB_398558
Anti-IL-17 (clone TC11-18H10)	BD Biosciences	Cat# 559502; RRID: AB_397256
Anti-Ki-67 (clone SolA15)	eBioscience	Cat# 17-5698-82; RRID: AB_2688057
Anti-KLRG-1 (clone 2F1)	BD Biosciences	Cat# 565393; RRID: AB_2739216

(*Continued on next page*)

Continued

REAGENT or RESOURCE	SOURCE	IDENTIFIER
Anti Ly-6A/E (SCA1) (clone D7)	BD Pharmingen	Cat# 560654; RRID: AB_1727552
Anti-Ly-6A/E (SCA1) (clone D7)	BioLegend	Cat# 108107; RRID: AB_313345
Anti-Ly-6C (clone AL-21)	BD Biosciences	Cat# 563011; RRID: AB_2737949
Anti-Ly-6G (clone 1A8)	BD Biosciences	Cat# 560602; RRID: AB_1727563
anti-Ly-6G (clone 1A8)	BioLegend	Cat# 127604; RRID: AB_1186105
Anti-MHC II, I-A/I-E (clone M5/114.15.2)	eBioscience	Cat# 56-5321-82; RRID: AB_494009
Anti-MHC II, I-A/I-E (clone M5/114.15.2)	BioLegend	Cat# 107635; RRID: AB_2561397
Anti-NK1.1 (clone PK136)	eBioscience	Cat# 48-5941-82; RRID: AB_2043877
Anti-NK1.1 (clone PK136)	eBioscience	Cat# 25-5941-82; RRID: AB_469665
Anti-NK1.1 (uncoupled, clone PK136)	eBioscience	Cat# 14-5941-85; RRID: AB_467737
Anti-NK1.1 (uncoupled, clone PK136)	BioLegend	Cat# 108760; RRID: AB_2800572
Anti-NKp46 (clone 29A1.4)	eBioscience	Cat# 46-3351-82; RRID: AB_1834441
Anti-PD-1 (clone J43)	eBioscience	Cat# 47-9985-82; RRID: AB_2574002
Anti-RORγt (clone B2D)	eBioscience	Cat# 46-6981-82; RRID: AB_10717956
CD1d/PBS57 Tetramer	NIH tetramer facilities	Cat# mCD1d PBS57
Streptavidin Pe-Cy5.5	eBioscience	Cat# 35-4317-82
Streptavidin APC-Cy7	eBioscience	Cat# 10-4317-82
Chemicals, peptides, and recombinant proteins		
Recombinant human Flt3-L	Amgen Inc. (Thousand Oaks, CA)[83]	Cat# CDX-301
Recombinant human Flt3-L	Miltenyi Biotec	Cat# 130-096-480
Sunitinib (Sutent)	Pfizer	Cat# NDC 0069-0550-38
Diphtheria Toxin	Sigma Aldrich	Cat# D0564-1MG
Zombie Red Fixable Viability Dye	BioLegend	Cat# 423103
eBioscience FoxP3 Staining Buffer Kit	Thermofisher	Cat# 50-112-8857
PMA (Phorbol 12-myristate 13-acetate)	Sigma-Aldrich	Cat# 16561-29-8
Ionomycin	Sigma-Aldrich	Cat# 56092-82-1
Collagenase D Type II	Roche	Cat# 11088882001
GolgiPlug	BD Biosciences	Cat# 555029
Critical commercial assays		
$CD4^+$ $CD25^+$ Regulatory T cell Isolation Kit, mouse	MACS Miltenyi Biotec	Cat# 130-091-041
Experimental models: Cell lines		
B16 melanoma	Olivier Lantz (Curie Institute, Paris, France)	Cat# CRL-6475; RRID: CVCL_0159
B16-FL melanoma	G. Dranoff (Dana-Farber Cancer Institute, Harvard Medical School, Boston, MA)[92]	RRID: CVCL_IJ12 PMID: 10866317
MC-38 colon carcinoma	Kerafast, Boston MA, USA	RRID: CVCL_B288
YUMM1.7 melanoma	Bosenberg (Yale University School of Medicine, New Haven, CT, USA)[97]	Cat# CRL-3362; RRID: CVCL_JK16 PMID: 27287723
Experimental models: Organisms/strains		
C57BL/6 mice	Janvier Labs	Cat#: C57BL/6JRj; RRID: IMSR_RJ:C57BL-6JRJ
	Jackson Labs	Cat# C57BL/6J RRID:IMSR_JAX:000664
	Charles River Laboratories	Cat# C57BL/6J (JAX® Mice Strain), Strain Code 632
NSG mice (NOD.Cg-*Prkdc*^{scid} *Il2rg*^{tm1Wjl}/SzJ)	Charles River Laboratories	Cat# 005557; RRID: IMSR_JAX:005557

(*Continued on next page*)

Continued

REAGENT or RESOURCE	SOURCE	IDENTIFIER
FL−/− mice	Paulo Vieira (Pasteur Institute, Paris, France) or Michel Nussenzweig (The Rockefeller University, New York, NY)	Cat# C57BL/6-flt3Ltm1Imx RRID:MMRRC_037395-JAX
zDC-DTR mice	Jackson Laboratory	Cat# B6(Cg)-Zbtb46tm1(HBEGF)Mnz/J RRID:IMSR_JAX:019506
Batf3−/− mice (Bone marrow cells)	François Xavier Mauvais (Institut Necker Enfants Malades, Paris, France)	RRID:IMSR_JAX:013755
CD45.1 C57BL/6 mice	Charles River Laboratories	Cat# B6.SJL-PtprcaPepcb/BoyCrl
Software and algorithms		
FlowJo version 10	BD Biosciences	N/A
PRISM version 9	GraphPad	N/A
R	CRAN	N/A
Other		
GDC Portal Data Repository	NIH	https://portal.gdc.cancer.gov

RESOURCE AVAILABILITY

Lead contact

Further information and requests should be directed to and will be fulfilled by the lead contact, Guillaume Darrasse-Jèze (guillaume.darrasse-jeze@inserm.fr).

Materials availability

This study did not generate new unique reagents.

Data and code availability

- Human cancer RNA-Seq data: survival and RNASeq data from both TCGA and TARGET cancer projects were freely downloaded from the GDC Cancer Portal of the National Cancer Institute (USA) (https://portal.gdc.cancer.gov/) (Files from release versions 11 and 12). Accession URL is also mentioned in the key resource table.
- Generation of cell subsets genes signatures: the following datasets accession numbers (NCBI GEO) were used to generate custom gene signatures for immune cell subsets: GSE94820, GSE35457, GSE80171, GSE89232,GSE6887, GSE60448, GSE24759, GSE65010 and GSE76598. See also Table S1.
- R code: the R code used to process and analyze these RNA-Seq data was directly generated from previously published R packages and methods such as *limma*, *DESeq2*, *survival*, *Rtsne*, *Bioconductor/GenomicDataCommons*, *survRM2*, *plot3D* and *XML*. These packages and their associated source code can be found either on CRAN or Bioconductor repositories. No new or original in-house algorithm or method were generated in this study.
- All data presented in this manuscript are available upon request to Dr. Darrasse-Jèze (guillaume.darrasse-jeze@inserm.fr).

EXPERIMENTAL MODELS AND SUBJECT DETAILS

Mice

FL$^{-/-}$ mice[8] were provided either by Paulo Vieira (Pasteur Institute, Paris, France) or Michel Nussenzweig (The Rockefeller University, New York, NY). *zDC*^{DTR} mice[154] were purchased from The Jackson Laboratory. NSG (NOD.Cg-*Prkdc*^{scid} *Il2rg*^{tm1Wjl}/SzJ) were purchased from Charles River Laboratories. C57Bl/6 mice were purchased from the Jackson Laboratory, Charles River laboratories or Janvier Labs. BM cells from *Batf3*$^{-/-}$ mice were provided by François Xavier Mauvais (Institut Necker Enfants Malades, Paris, France). CD45.1 C57Bl/6 congenic mice were maintained in our facility. All mice used were 7–12 weeks-old females and were maintained in specific pathogen-free conditions. Mice compared in each experiment were from the same commercial origin and were cohoused to minimize the influence of gut microflora.[155] Similar results were obtained using male or female mice. All mice were treated in accordance with the European Union guidelines for animal experimentation and National Institutes of Health guidelines, and were approved by the Ministère de l'Enseignement Supérieur, de la Recherche et de l'Innovation – France (APAFIS# 29416)

Cell lines

The highly tolerogenic B16 tumor cell line, derived from a C57Bl/6 melanoma (CRL-6475), was provided by Olivier Lantz (Curie Institute, Paris, France). The B16-FL tumor cell line (CVCL_IJ12), a kind gift of M. Nussenzweig, was obtained from G. Dranoff

(Dana-Farber Cancer Institute, Harvard Medical School, Boston, MA; USA[89]). The doubling time and cell death of these two cell lines in *in-vitro* culture were not significantly different in our hands as well as in the hands of other authors.[102] YUMM1.7[92] (CRL-3362) cells were obtained from ATCC. The MC38 cell line (CVCL_B288) was obtained from Kerafast (Boston, MA, USA). All cell lines were cultured in DMEM (Invitrogen) complemented with 10% FCS, 2 mM L-glutamine (Invitrogen), and 100 U/mL penicillin-streptomycin (Invitrogen) at 37°C, 5% CO_2. All cell lines were mycoplasma-free.

Subjects

The study was entirely computational and did not involve human subjects as it obtained data neither through intervention nor interaction with living individuals nor contains identifiable private information. The human results reported here exclusively used anonymized data available from the GDC Cancer Portal of the National Cancer Institute (USA) (https://portal.gdc.cancer.gov/), generated by the TCGA (The Cancer Genome Atlas) and TARGET (Therapeutically Applicable Research to Generate Effective Treatments) Research Networks: https://www.cancer.gov/ccg/research/genome-sequencing.

METHOD DETAILS

In vivo mouse tumor models

For *in-vivo* experiments, 5×10^5 B16, B16-FL, YUMM1.7 or MC38 tumor cells were injected *s.c.* in the left flank of a mouse. Mean tumor diameter was determined by measuring perpendicular tumor diameters using vernier calipers. Mouse survival was monitored daily. Survival was determined by the time at which mice required euthanasia, when tumor ulcerated and/or mean diameter reached 15 mm. Of note, we never observed presence of B16 cells in the LN.

Treatments

Recombinant human FL (rFL) was obtained from Amgen or Miltenyi Biotech. For rFL injection, 10 μg recombinant human FLT3-L (Amgen) in 100 μL PBS was injected subcutaneously every other day, for 20 days, beginning 4 days prior to the tumor injection (unless otherwise stated).

Mice were gavaged with 40 mg/kg sunitinib (Sutent; Pfizer) via feeding needles (Popper) every day for 7 days, beginning 3 days before tumor injection.

During survival experiments, some mice received 2 intraperitoneal injections of depleting anti-NKs antibodies in a volume of 250 μL at the day of tumor injection (d0) and at d5 after tumor inoculation either anti-NK1.1 (300 μg per injection, clone PK136 from either eBioscience or Biolegend) or anti-Asialo-GM1 (100 μL per injection, clone Poly21460 from BioLegend) or an isotypic control (300 μg per injection, Purified Mouse IgG2a, κ isotype Ctrl MOPC from Biolegend). Of note, mice treated with isotype control, PBS, did not differ from untreated (not shown). For T cell depletion, mice were treated at d4 of tumor growth by anti-CD4 (clone GK1.5) and anti-CD8 (clone 53–6.7) depleting antibodies (500 μg each per mice). For ICB therapies, mice were treated at d5, d8 and d11 by anti-CTLA4 (100 μg per injection, clone 9H10, Biolegend) and/or anti-PD1 (250 μg per injection clone 29F.1A12, Biolegend) antibodies.

BM chimeras were reconstituted for at least 8–10 weeks after lethal irradiation (two doses of 525 rad, 3 h apart) and *i.v.* transfer of $5\text{-}10 \times 10^6$ BM cells 3 h later.

Cells preparation

Organs were gently dispersed between frosted slides and were digested for 30 min at 37°C in RPMI 1640 medium (Invitrogen) with 10% (v/v) FCS-containing collagenase D (type II; Roche) at a final concentration of 0.4 U/mL. For disruption of DC-T cell complexes, 200 μL of 0.5 M EDTA, pH 8.0, was added for 5 min. Remaining pieces were gently dissociated between frosted slides. All subsequent steps were at 4°C with 5% (v/v) FBS in PBS. Cells were passed through a 70 μm cell strainer and washed in 5% (v/v) FBS in PBS. Cell numbers were determined with a FACS Fortessa (BD).

Immune cells phenotyping and flow cytometry analysis

The following antibodies from either BD Biosciences, eBioscience or BioLegend were used: anti-CD3ε (145-2C11), CD4 (RM4-5), CD8α (53–6.7), CD11b (M1/70), CD11c (HL3), CD19 (1D3), CD25 (PC61), CD40 (HM40-3), CD44 (IM7), CD69 (H1.2F3), CD86 (GL1), CD103 (M290), CD206 (C068C2), CTLA-4 (UC10-4F10-11), DC-SIGN (MMD3), EpCAM (G8.8), F4/80 (BM8), Foxp3 (FJK-16s), IFNγ (XMG1.2), IL-2 (JES6-5H4), IL-10 (JSE5-16E3), IL-17 (TC11-18H10), Ki-67 (SolA15), KLRG-1 (2F1), Ly-6C (AL-21), Ly-6G (1A8), MHC II (M5/114.15.2), NK1.1 (PK136), NKp46 (29A1.4), PD-1 (J43), IL-10 (JSE5-16E3) and IFNγ (XMG1.2). Isotype-irrelevant mAbs were used as controls. FcBlock (BD Pharmingen) and Zombie Red Fixable Viability Kit (BioLegend) were used following the manufacturer's recommendations.

For iNKT tetramer staining, tetramer was added concomitantly with purified anti CD16/CD32 on resuspended cells for 45 min at room temperature in the dark. Gating strategy for iNKT and ILCs are available in Figures S4A and S4D.

Intracellular labeling of Ki-67, FoxP3, Eomes, RoRγt CD206 and DC-SIGN were performed using eBioscience FoxP3 Staining Buffer kit (Invitrogen - Thermofisher) according to the manufacturer's recommendations.

For intracellular cytokine staining, cells were incubated at 37°C, 5% CO_2 for 6 h in 10% FCS complete RPMI 1640 medium with 1 μg/mL PMA (Sigma-Aldrich), 750 ng/mL ionomycin (Sigma-Aldrich) and 1 μL/mL GolgiPlug (BD) which was added after 45 min.

Surface staining was performed for 30 min, after which the cells were resuspended in fixation/permeabilization solution (eBioscience FoxP3 Staining Buffer kit, Invitrogen - Thermofisher). Intracellular cytokine staining was performed according to the manufacturer's protocol.

Processed cells were analyzed by 17 parameters flow cytometry on a BD LSR Fortessa. Further analyses were performed with FlowJo software (FlowJo, LLC). Finally, PZC format coded scripts were used to link FlowJo-exported data to Prism (GraphPad Software) workspaces for statistical analysis.

t-SNE plots were generated with R scripts adapted from the original description of the t-SNE algorithm by L.J.P. van der Maaten (https://lvdmaaten.github.io/tsne/): recommended parameters were used and each plot represents the pool of each replicate of the corresponding situation, in order to avoid computational and statistical bias during the random subsampling.

CFSE staining and adoptive transfers of cells.

$CD4^+$ $CD25^{hi}$ Tregs were FACS-sorted (FACS Aria II) from MACS-sorted (Miltenyi Biotec) $CD4^+$ T_{cells} from pooled LNs and spleens from CD45.1 congenic mice. Tregs were then labeled with CFSE (Sigma-Aldrich) and immediately transferred intravenously after purity checking by flow cytometry. In host mice, the transferred T_{cells} were later identified by the expression of CD3, CD4, FoxP3 and CD45.1 and CD45.2. After adoptive transfer in WT hosts under our experimental conditions (Fisson et al., 2003), donor $CD45.1^+$ Treg cells represented 0.1% of splenocytes. Therefore, 2-5 × 10^6 events were acquired for each analysis.

Bioinformatic analysis of cancer patient data

Survival and RNASeq data from both The Cancer Genome Atlas (TCGA) and TARGET (Therapeutically Applicable Research to Generate Effective Treatments) cancer projects available from the GDC Cancer Portal of the National Cancer Institute (USA) (https://portal.gdc.cancer.gov/) (Files from release versions 11 and 12) were downloaded, normalized using the R package DEseq2 and further analyzed through R.

The TCGA and TARGET projects selected cancers based on specific criteria available here: https://www.cancer.gov/ccg/research/genome-sequencing/tcga/studied-cancers and here: https://www.cancer.gov/ccg/research/genome-sequencing/target/studied-cancers respectively. These pages contain links to each individual study included in the projects. We used all (anonymized) RNA-seq data freely available from these databases. 35 Cancer types presented beneficial, detrimental or paradoxical role of gene or gene signature on survival, other cancer types did not. The precise number of patients for each cancer type is indicated in figures 6 and S6.

Algorithmic determination of patients cutoffs: To determine the low, intermediate and high patients groups for the expression of a given gene/gene signature, we constructed the survival curves opposing patients with lower or higher gene expression values vs. the remaining patients for every percentile between 1% and 33% and we calculated the Log rank test associated χ^2 statistics for each percentile. Then, we chose the low and high cutoffs corresponding to the best $\chi 2$ statistic (Table S1). A given gene was classified by an R script as beneficial (correlation), detrimental (inverse correlation) or paradoxical for a cancer type, according to the area under the curve (AUC) estimation of hi, inter and lo survival curves.

Calculation of genes signatures scores: For a given gene signature, we established for each patient an associated Quantitative Score (QS) by calculating the arithmetic mean of all the normalized and background-corrected gene expression values for each of the genes in the given signature.

Generation of cell subsets genes signatures: To generate custom gene signatures for immune cell subsets (Table S1), we used raw transcriptomic data available in NCBI's Gene Expression Omnibus (GEO: GSE94820, GSE35457, GSE80171, GSE89232, GSE6887, GSE60448, GSE24759, GSE65010 and GSE76598) and processed-data from literature.[156–163] We then reanalyzed these data and compared them by Venn diagrams to finally only choose the genes that are specific of each signature.

QUANTIFICATION AND STATISTICAL ANALYSIS

Statistical analyses of the survival curves were performed using Log rank (Mantel-Cox) tests. Comparisons of one-parameter data were performed using two-tailed unpaired Student t-tests after ensuring with Shapiro-Wilk tests that corresponding data follow a normal distribution. Statistical significances were evaluated with the Prism software (GraphPad). Data shown and error bars are expressed as means ± SEM, and a p value<0.05 (eventually after Holm-Sidak correction) was considered as significant. For all tests, *: $p < 0.05$, **: $p < 0.01$, ***: $p < 0.001$, ****: $p < 0.0001$. Details about the compared groups are indicated in each figure. Other statistical details including sample size can be found in figure legends. Noteworthily, regarding the human RNA-Seq data from TCGA dataset, we used the standard modeling and differential analysis protocol described by the limma R package authors (available in the corresponding documentation, PMID: 25605792) which is able to analyze both microarrays and RNA-Seq data.

Cell Reports Medicine, Volume *4*

Supplemental information

FLT3L-dependent dendritic cells control tumor immunity by modulating Treg and NK cell homeostasis

Paul Régnier, Mathias Vetillard, Adèle Bansard, Eméranne Pierre, Xinyue Li, Nicolas Cagnard, Emmanuel L. Gautier, Pierre Guermonprez, Bénédicte Manoury, Katrina Podsypanina, and Guillaume Darrasse-Jèze

SUPPLEMENTAL TEXT and FIGURES

FLT3L-dependent Dendritic Cells Control Tumor Immunity by Modulating Treg and NK Cell Homeostasis

Paul Régnier[1,2,3], Mathias Vetillard[4], Adèle Bansard[1,5], Eméranne Pierre[5], Xinyue Li[2], Nicolas Cagnard[6], Emmanuel L. Gautier[7], Pierre Guermonprez[4,8], Bénédicte Manoury[1], Katrina Podsypanina[1,9,10], Guillaume Darrasse-Jèze[1,2,5 *],
1: Institut Necker Enfants Malades, INSERM U1151-CNRS UMR 8253, Université de Paris Cité, Faculté de Médecine Necker, Paris, France.
2: Sorbonne Université, INSERM, UMR S 959, Immunology-Immunopathology- Immunotherapy (I3), F-75005, Paris, France.
3: AP-HP, Groupe Hospitalier Pitié-Salpêtrière, Department of Internal medicine and clinical immunology, DMU3ID, F-75013, Paris, France.
4: Université de Paris Cité, INSERM U1149, CNRS erl8252, Centre for Inflammation Research, Université de Paris Cité, Paris, France.
5: Université Paris Cité, Faculté de Médecine Paris Descartes, Paris, France.
6: Structure Fédérative de Recherche (SFR) Necker, Université Paris Descartes, Paris France
7: Institut National de la Santé et de la Recherche Médicale (Inserm, UMR-S 1166), Sorbonne Université, Hôpital de la Pitié-Salpêtrière, Paris, France.
8: Institut Pasteur, Paris, France
9: Institut Curie, PSL Research University, CNRS, UMR3664, Paris, France.
10: Sorbonne Université, UPMC Univ Paris 06, CNRS, UMR3664, Paris, France.

Content :

* Corresponding author

Supplementary Discussion

Graphical Abstract description:

Proposed model of FL influence on homeostatic interactions between DCs, Tregs, effector T cells and NK cells during cancer. In the steady state, tissue self-Ag, originating from dying cells, molecule shedding, or direct capture from live cells, are presented by DCs in the dLNs. This presentation of self-antigens induces activation of specific autoreactive regulatory (Tregs) and effector (Teff) T cells, which is sustained by the subsequent production of IL-2[1*]. This phenomenon is amplified during tumor development. In the absence of additional activation stimuli, increased number of DCs drives more tTregs recruitment (Fig.1A of the article) *via* tumor-self Ag presentation in a MHC-II-dependent fashion[2,3], and favors early establishment of immune tolerance to a tumor, keeping in check anti-tumor immune responses[4]. Low levels of FL expression lead to a decrease in DCs, which in turn results in a fall in the number of Tregs[5] and favors the recruitment of Teffs that appear to be less dependent on cDCs than Tregs (Fig.2,[5,6]). DC decrease also reduces the number of NK_{cells}, as they appear essential to their homeostasis (Fig.3), likely by a mechanism involving IL-15 trans-presentation[7]. Tumor cells in this context will thus face an enhanced adaptive immune response and a decreased NK_{cell}-mediated innate response. Conversely, a FL^{high} context will boost NK_{cells} and Tregs, the latter causing a relative decrease in Th cell activation, resulting in an anti-tumor immune response fueled mainly by NK_{cells} as well as $CD8^{+}T_{cells}$ (Fig.3), which will also stimulate the recruitment of DC1 into the tumor microenvironment promoting cancer immune control[8].

[*] The references are in the main text

Table S2: Abbreviations related to the manuscript and the STAR Methods

BM: Bone marrow

CDP: common dendritic progenitor

CTLs: cytotoxic T cells ($CD8^+$T cells)

CTLA-4: cytotoxic T-lymphocyte-associated protein 4 (CD152)

DC: Dendritic cell

DC1: rDC1 and mDC1 (come from the same CDP progenitor subset in the bone marrow)

DC2: rDC2 and mDC2 (come from the same CDP progenitor subset in the bone marrow)

DMD: Duchenne muscular dystrophy gene (dystrophin)

cDC: FLT3L-dependent $Zbtb46^+$ 'classical' dendritic cells derived from the CDP precursor in the bone marrow

rDC1: LN-resident 'classical' dendritic cell type 1 ($CD11b^{-/int}$ $CD8^+$ in mice; $XCR1^+$ $CD141^+$ in humans)

rDC2: LN-resident 'classical' dendritic cell type 2 ($CD8^-CD11b^+$ in mice; $CD1c^+$ in humans)

LNs: lymph nodes

dLNs: tumor-draining lymph nodes

DT: diphtheria toxin

DTR: diphtheria toxin receptor

infMo: Inflammatory monocytes

LCs: Langerhans cells

Lang: Langerin

FL: Flt3 ligand (*FLT3LG* gene)

Flt3: Fms-like tyrosine kinase 3 receptor (*FLT3* gene)

$FL^{-/-}{}_{B16}$: C57Bl/6 *Flt3-L*$^{-/-}$ mice injected *s.c.* with 0.5M of B16-F10 melanoma cells

Fms: Type III receptor tyrosine kinase that binds to the macrophage or monocyte colony-stimulating factor (M-CSF or CSF-1). Oncogene responsible for Feline McDonough Sarcoma.

IC: immune checkpoints

ICB: immune checkpoints blockade

ICBT: immune checkpoints blockade therapy

IL-2: interleukin 2

IL-15: interleukin 15

LNs: lymph nodes

MDP: macrophage/dendritic progenitors

mDC1: Migratory 'classical' dendritic cell type 1 ($CD11b^-$ $CD103^+$ $Epcam^+$ in mice; $XCR1^+CD141^+$ in humans)

mDC2: Migratory 'classical' dendritic cell type 2 ($CD103^-Epcam^{-/lo}CD11b^+$ in mice; $CD14^-$ $CLEC10A^+CD1c^+$(BDCA-1^+) in humans)

NK cells: natural killer cells

NSG_{B16}: NSG mice injected s.c. with $0.5x10^6$ of B16-F10

$NSG_{B16\text{-}FL}$: NSG mice injected s.c. with $0.5x10^6$ of B16-FL melanoma cells genetically engineered to constitutively express Flt3-L (B16-FL)

PD-1: Programmed cell death protein 1 (CD279)

rFL: recombinant FL

resMo: Resident monocytes

s.c: subcutaneously

Teffs: effector T cells

Th: helper $CD4^+$ $Foxp3^-$ T cells

Treg: $CD4^+$ $Foxp3^+$ regulatory T cells

t-SNE: t-distributed stochastic neighbor embedding

WT_{B16}: C57Bl/6 WT mice injected s.c. with 0.5×10^6 of B16-F10 melanoma cells

$WT^{+rFL}{}_{B16}$: C57Bl/6 WT mice injected s.c. with 0.5×10^6 of B16-F10 melanoma cells and regularly injected with rFL

$WT_{B16\text{-}FL}$: C57Bl/6 WT mice injected s.c. with 0.5×10^6 of B16-F10 melanoma cells genetically engineered to constitutively express Flt3-L (B16-FL)

zDC: Zbtb46 (Zinc Finger And BTB Domain Containing 46) (*ZBTB46* gene)

Fig. S1

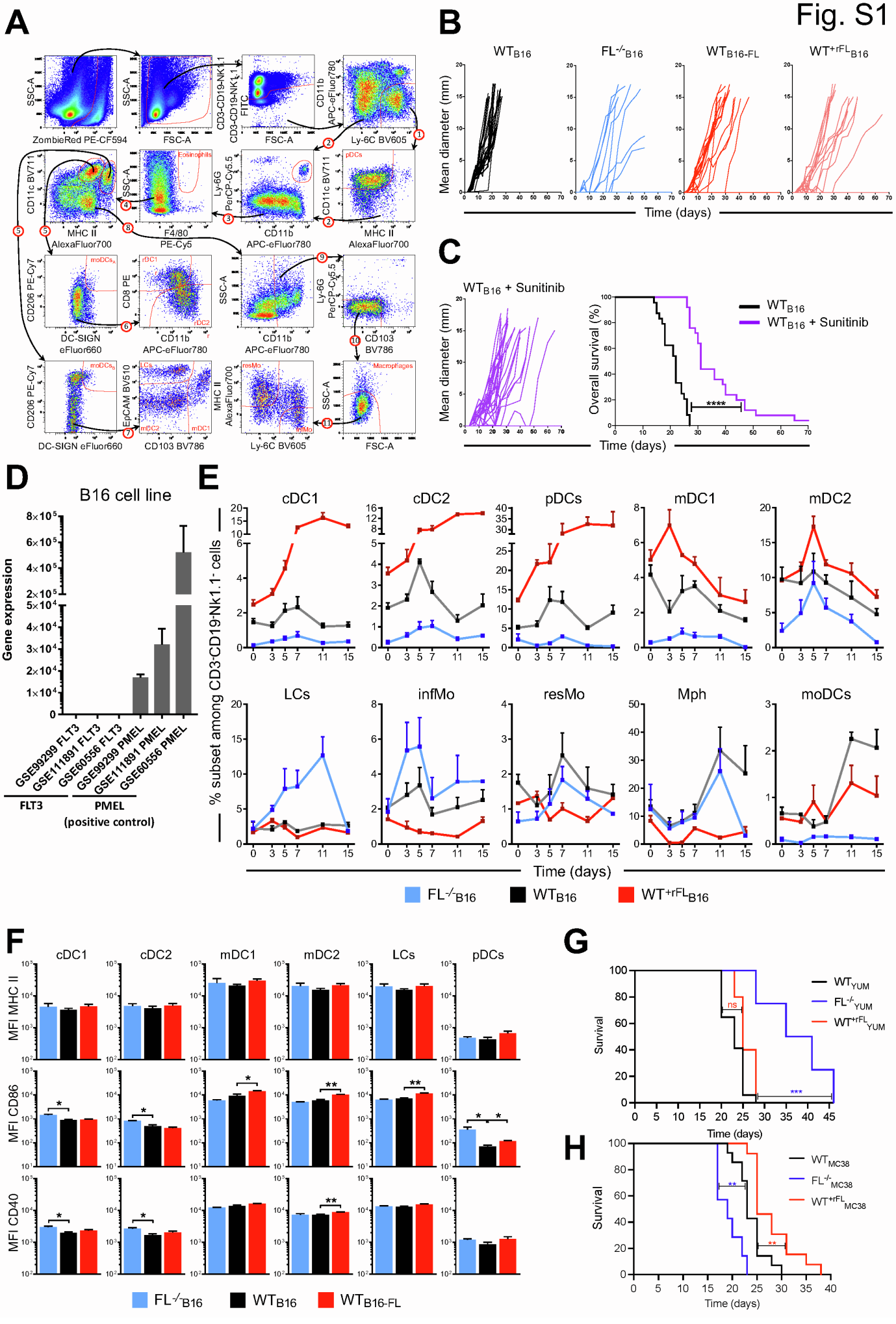
A
B
C
D
E
F
G
H
Mean diameter (mm)
Time (days)
Overall survival (%)
Gene expression
% subset among CD3-CD19-Nk1.1- cells
MFI MHC II
MFI CD86
MFI CD40
Survival
FLT3
PMEL
(positive control)
cDC1
cDC2
pDCs
mDC1
mDC2
LCs
infMo
resMo
Mph
moDCs

Figure S1. FL levels affect DC frequencies, tumor growth and survival of tumor-bearing mice. Related to Figure 1.

(A) General gating strategy used to analyze dendritic cells and the myeloid and granulocytic compartments of the tumor-draining lymph nodes and the tumor site (adapted from [159]).

Sequentially, we first gated for live cells by excluding those with a positive ZombieRed signal, followed by the selection of lymphoid and myeloid-shaped single cells (removal of cell doublets using H and W vs A parameters of FSC and SSC is not shown). Subsequently, we further excluded $CD3^+$, $CD19^+$, and $NK1.1^+$ cells. Among the $CD3^-CD19^-NK1.1^-$ cells we gated on $Ly6C^+CD11b^-$ cells and identified pDCs among them as $CD11c^+$ $MHCII^{lo/int}$ **(1)**. Using boolean gates we identified neutrophils as $Ly\text{-}6G^+$ $CD11b^+$ cells among non-pDCs CD3-CD19-NK1.1- cells **(2)**. Subsequently, eosinophils were identified as $SSC\text{-}A^{hi}$ $F4/80^{int}$ cells among the non-neutrophil population **(3)**. For the remaining cells, we defined two major subsets of dendritic cells (DCs), namely global resident DCs (rDCs) and migratory DCs (mDCs), based on their expression of CD11c and MHC II. Specifically, rDCs were identified as $CD11c^{hi}$ MHC II^+ cells, while mDCs were characterized as $CD11c^{+/hi}$ MHC II^{hi} cells **(4)**. Within these global rDCs and mDCs gates, we identified a distinct population of monocyte-derived DCs (moDCs) as DC-$SIGN^+$ $CD206^+$ cells (sum of $moDCs_A$ and $moDCs_B$ on the panel and considered as a unique population) **(5)**. Within the non-moDCs remaining cells among the rDCs gate, we further classified two subsets: rDC1 ($CD8^+$ $CD11b^{lo/+}$) and rDC2 ($CD8^-$ $CD11b^{+/hi}$) classical dendritic cells **(6)**. Within the global mDCs gate, we identified three subsets among non-moDCs: Langerhans cells (LCs) ($CD103^{-/lo}$ $EpCAM^{hi}$), mDC1 ($CD103^+$ $EpCAM^{int}$) and mDC2 ($CD103^{-/lo}$ $EpCAM^-$) **(7)**. Of note, all mDC2 cells are $CD11b^+$ (not shown). In parallel, within the remaining cell population not assigned to global rDCs or mDCs **(8)**, we gated for $CD11b^+$ cells and further excluded cells expressing either Ly6G or CD103 **(9)**. These remaining cells were classified as macrophages based on their high scatter parameters ($SSC\text{-}A^{int/hi}$) **(10)**. Finally, within the cell population not identified as macrophages, we distinguished resident monocytes (resMo) as MHC II^+ $Ly\text{-}6C^-$ cells, and inflammatory monocytes (infMo) as MHC II^- $Ly\text{-}6C^+$ cells **(11)**. Accordingly, each studied myeloid population in the manuscript can be identified as follows:

rDC1 (resident cDC1): $CD3^-CD19^-NK1.1^-$ $Ly6G^-$ $(CD206^+DC\text{-}SIGN^+)^-$ $CD11c^{hi}MHCII^+$ $CD11b^-$ $CD8^+$

rDC2 (resident cDC2): $CD3^-CD19^-NK1.1^-$ $Ly6G^-$ $(CD206^+DC\text{-}SIGN^+)^-$ $CD11c^{hi}MHCII^+$ $CD8^-$ $CD11b^+$),

mDC1 (migratory cDC1): $CD3^-CD19^-NK1.1^-$ $Ly6G^-$ $CD11c^+MHCII^{hi}$ $(CD206^+DC\text{-}SIGN^+)^-$ $EpCAM^{int}$ $CD11b^-$ $CD103^+$ (they are also $Ly6C^-$ $CD8^{-/lo}$ not shown),

mDC2 (migratory cDC2), $CD3^-CD19^-NK1.1^-$ Ly6G- $CD11c^+MHCII^{hi}$ $(CD206^+DC\text{-}SIGN^+)^-$ $CD103^-EpCAM^-$ (they are also $Ly6C^-$ $CD11b^+$, not shown),

pDCs (plasmacytoid DCs, $CD3^-CD19^-NK1.1^-$ $CD11b^-$ $Ly6C^+$ $CD11c^+$),

moDCs (monocyte-derived DCs): $CD3^-CD19^-NK1.1^-$ $Ly6G^-$ $CD11c^+MHCII^{+/hi}$ $CD206^+$ $DC\text{-}SIGN^+$,

LC (Langerhans cells): $CD3^-CD19^-NK1.1^-$ $Ly6G^-$ $(CD206^+DC\text{-}SIGN^+)^-$ $CD11c^+MHCII^{hi}$ $CD103^-EpCAM^+$ (they are also $CD11b^+$ $Ly6C^{-/lo}$ not shown),

resMo (resident monocytes): $CD3^-CD19^-NK1.1^-$ $CD11c^{-/int}$ $CD11b^+$ $Ly6G^-CD103^-$ $SSC^{lo}FSC^{lo}$ $Ly6c^{-/lo}MHCII^+$,

infMo (inflammatory monocytes): $CD3^-CD19^-NK1.1^-$ $CD11c^{-/int}$ $CD11b^+$ $Ly6G^-CD103^-$ $SSC^{lo}FSC^{lo}$ $MHCII^{-/lo}$ $Ly6c^{hi}$),

Macrophages: $CD3^-CD19^-NK1.1^-$ $CD11c^{-/int}$ $CD11b^+$ $Ly6G^-$ $CD103^-$ $SSC^{int/hi}FSC^{int/hi}$,

Neutrophils: $CD3^-CD19^-NK1.1^-$ CD11b+ $Ly6G^+$ (they are also $Ly6C^{int}$, SSC^{int} not shown),

Eosinophils: $CD3^-CD19^-NK1.1^-$ CD11b+ $F4/80^{int}$ SSC^{hi} (they are also $Ly6c^{-/lo}LY6G^-$ not shown).

(B) Graphs show the individual tumor growth of the indicated groups of mice depicted in Fig.1B.

(C) Mean tumor diameter (left) and Kaplan-Meyer plot (right) showing tumor growth and overall survival of B6 mice treated with Sunitinib (WT_{B16}+ Sunitinib, purple, n=25, 3 experiments pooled, Log-rank test difference with WT_{B16}: $p<0.0001$).

(D) Expression of *FLT3* and *PMEL* (positive control) genes in several B16 melanoma cells samples coming from 3 different indicated RNASeq experiments.

(E) Graphs show the actual frequencies at different timepoints after tumor inoculation of DCs and myeloid populations among the $CD3^-CD19^-NK1.1^-$ subset in the dLNs from $FL^{-/-}$ and FL-overexpressing tumor-bearing mice (n=5-15 mice per timepoint).

(F) Histograms showing the MFI of MHC II, CD86 and CD40 on the surface of several DCs subsets related to the indicated groups of mice depicted in Fig.1D (n=3, same mice as in Fig.1C).

(G) Kaplan-Meyer plot showing survival of YUMM1.7-bearing FL-deficient ($FL^{-/-}{}_{YUM}$, blue, n=4, Log-rank test difference with WT_{YIM}: $p<0.0007$), and FL-overexpressing mice ($WT^{+rhFL}{}_{YUM}$, red, n=5, $p<0.0529$) over control animals (WT_{YUM}, black, n=17) (2 experiments pooled representatives of 3).

(H) Kaplan-Meyer plot showing survival of MC38-bearing FL-deficient ($FL^{-/-}{}_{MC38}$, blue, n=7, Log-rank test difference with WT_{MC38}: $p<0,0012$), and FL-overexpressing mice ($WT^{+rhFL}{}_{MC38}$, red, n=13, $p<0.0033$) over control animals (WT_{MC38}, black, n=14) (2 experiments pooled representatives of 4).

Fig. S2

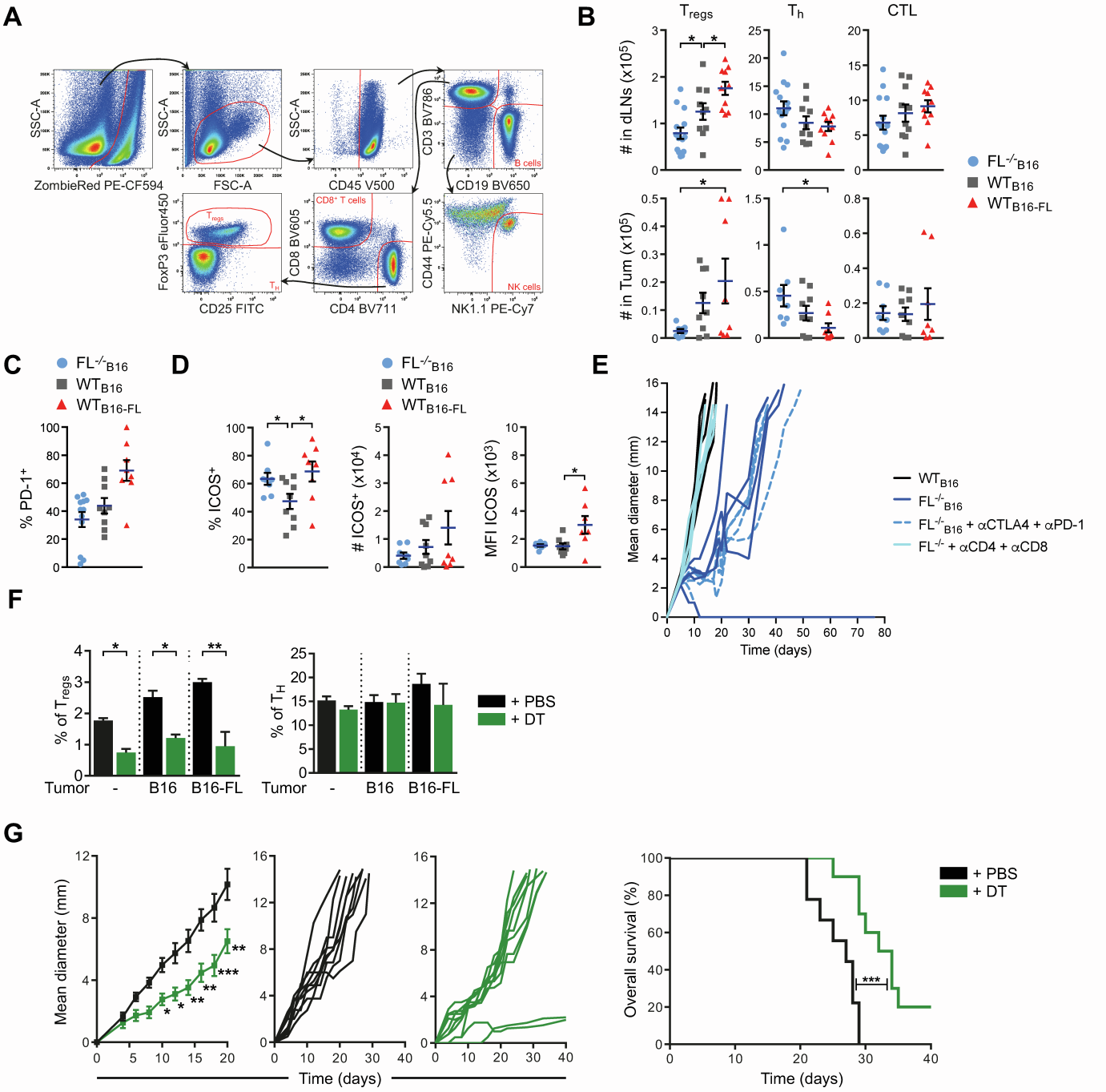

Figure S2. Dendritic cells levels affect frequencies and anti-tumor activity of Tregs and Teffs cells in tumor and dLN. Related to Figures 2, 3 and 5. (A) Gating strategy used to analyze the lymphocytic compartments of the tumor-draining lymph nodes and the tumor site. After dead cell removal, cell size gating and removal of doublets as depicted for DCs/myeloid cells (Fig.S1A), mentioned populations were gated as shown in the graph: Tregs ($CD45^+CD3^+CD19^-CD4^+Foxp3^+$), Th cells ($CD45^+CD3^+CD19^-CD4^+Foxp3^-$), NK cells ($CD45^+CD3^-CD19^-NK1.1/NKP46^+$), CD8 T cells ($CD45^+CD3^+CD19^-CD4^-CD8^+$). **(B)** Scatter plots show the absolute numbers of Tregs, Th and CTL related to the indicated groups of mice depicted in Fig.2A. **(C-D)** Scatter plots show the expression of PD1 **(C)** or ICOS **(D)** by Tregs from dLNs related to the indicated groups of mice depicted in Fig.2A **(E)** Individual tumor growth of the indicated groups of mice depicted in Fig.2F: Mean tumor diameter of each mouse is shown (n= 5 mice per group, one experiment representative of 2 is shown). **(F)** Tregs and Th cell frequencies at day 11 after tumor cell inoculation in dLNs of B16 or B16-FL tumor-bearing *zDC^{DTR}* chimeras mice treated with PBS or DT, as depicted in Fig.5C. **(G)** Tumor mean diameter (by groups and individualized, top) and survival curves (bottom) of tumor-bearing *zDC^{DTR}* chimeras mice treated with PBS (n=9) or DT (n=10). Log-rank test difference was performed.

Fig. S3

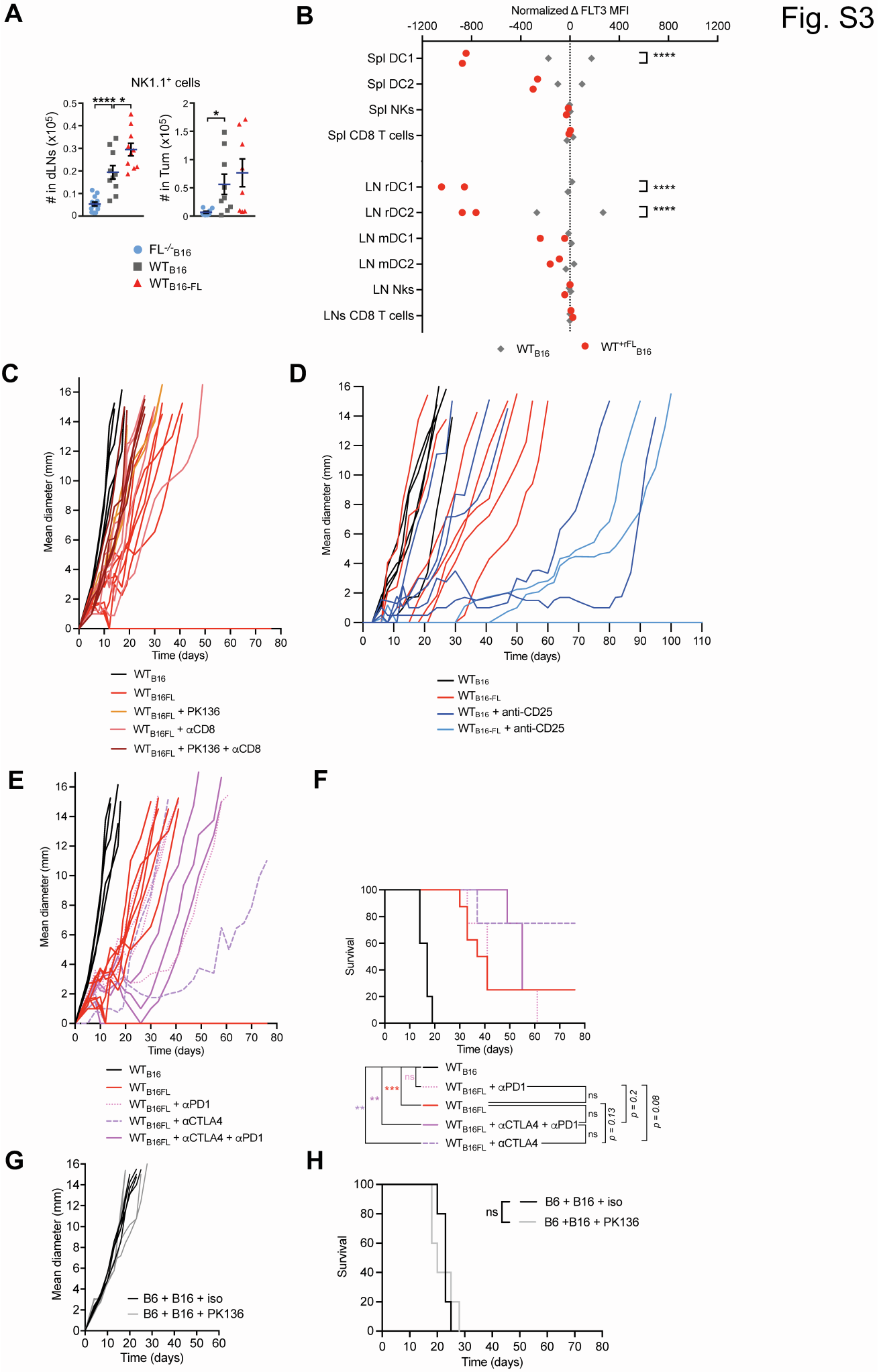
A
NK1.1+ cells
in dLNs (x10^5)
in Tum (x10^5)
FL-/- B16
WT B16
WT B16-FL
B
Normalized Δ FLT3 MFI
Spl DC1
Spl DC2
Spl NKs
Spl CD8 T cells
LN rDC1
LN rDC2
LN mDC1
LN mDC2
LN Nks
LNs CD8 T cells
WT B16
WT +rFL B16
C
Mean diameter (mm)
Time (days)
WT B16
WT B16FL
WT B16FL + PK136
WT B16FL + αCD8
WT B16FL + PK136 + αCD8
D
Mean diameter (mm)
Time (days)
WT B16
WT B16-FL
WT B16 + anti-CD25
WT B16-FL + anti-CD25
E
Mean diameter (mm)
Time (days)
WT B16
WT B16FL
WT B16FL + αPD1
WT B16FL + αCTLA4
WT B16FL + αCTLA4 + αPD1
F
Survival
Time (days)
WT B16
WT B16FL + αPD1
WT B16FL
WT B16FL + αCTLA4 + αPD1
WT B16FL + αCTLA4
p = 0.13
p = 0.2
p = 0.08
G
Mean diameter (mm)
Time (days)
B6 + B16 + iso
B6 + B16 + PK136
H
Survival
Time (days)
B6 + B16 + iso
B6 +B16 + PK136

Figure S3. FL overexpression favors in-vivo recruitment and anti-tumor activity of NK cells and synergizes with Treg depletion or anti-CTLA4 ICB to improve mouse survival. Related to Figure 3.

(A) Scatter plots show the absolute numbers of NK cells related to the indicated groups depicted in Fig.3A. Groups were compared using t-tests.

(B) Effect of FL abundancy on the expression of FLT3: Scatter plots show the difference of FLT3 expression in DC1, DC2, CD8 T cells and $NK1.1^+$ cells of the spleen and cutaneous LN from mice treated daily with recombinant FL for 7 days. Data were normalized to the average geometric mean fluorescence index of the untreated group (assigned as 0). Groups were compared using one-way Anova tests.

(C) Graphs show the individual tumor growth of the indicated groups of mice depicted in Fig.3F. Mean tumor diameter (left) of B16 or B16FL tumor-bearing B6 mice non-treated or treated with anti NK1.1 (PK136), antiCD8 (53-6.7) or both (WT_{B16}+ Sunitinib, purple, (n=4 - 8 mice per group).

(D) Graphs show the individual tumor growth of the indicated groups of mice depicted in Fig.3G. Mean tumor diameter (left) of B16 or B16FL tumor-bearing B6 mice non-treated or treated with anti CD25 (PC61), (n=5 - 10 mice per group).

(E-F) Graphs show the tumor growth **(E)** and the overall survival **(F)** of B16 or B16-FL tumor-bearing mice treated or not with anti-PD-1 (29F.1A12), anti CTLA4 (9H10) or both (n=4 - 8 mice per group). Survival curves were compared using Log-rank tests. Of note, results shown in (C) and (E-F) were obtained during the same experiment.

(G-H) Graphs show the tumor growth **(G)** and the overall survival **(H)** of B16 tumor-bearing mice treated or not with anti-NK1.1 (PK136) or isotypic control antibody (n=5 mice per group). Survival curves were compared using Log-rank tests.

*: p-value<0.05, **: p-value<0.01, ***: p-value<0.001, ****: p-value<0.0001.

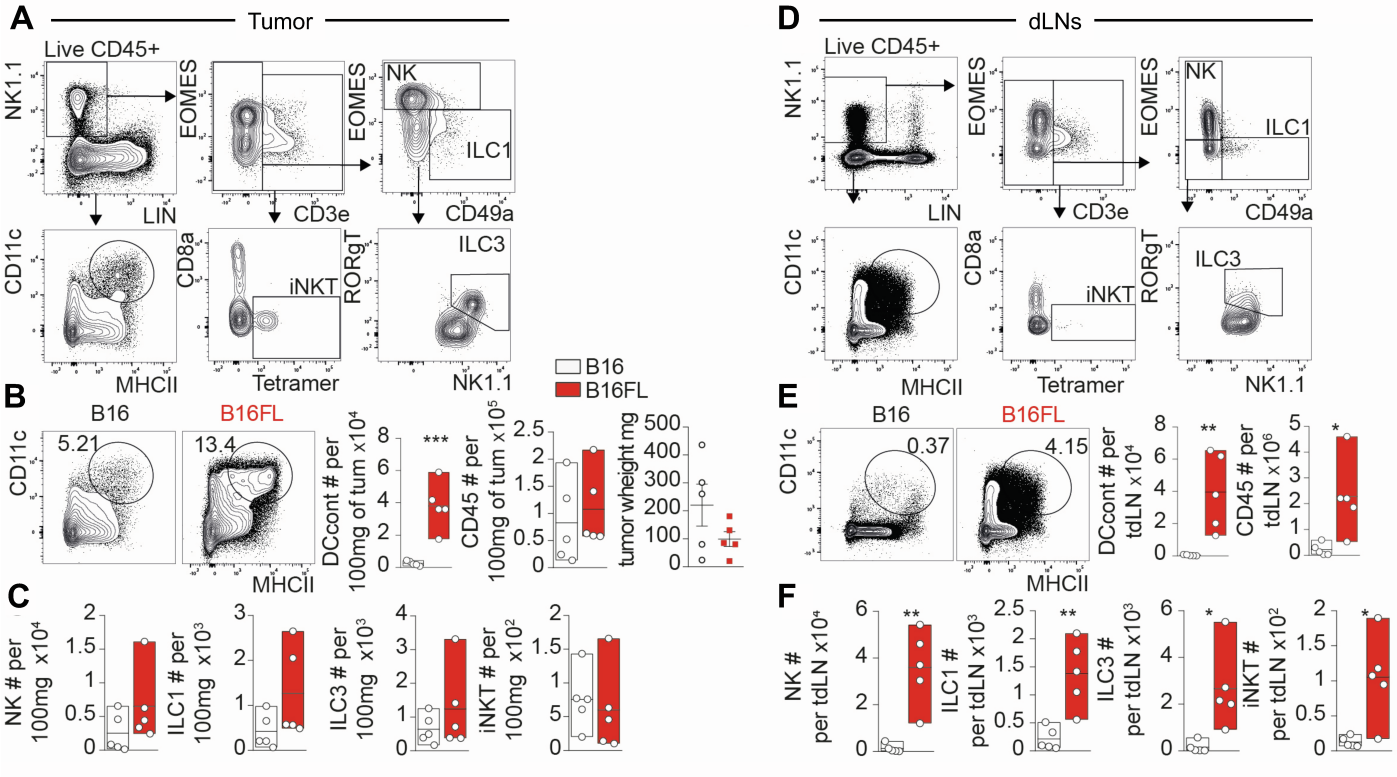

Figure S4. NK1.1^{+} cells recruited to tumors and dLNs in the FL^{hi} setting are mainly NK cells. Related to Figure 4.

(A) Gating strategy for NK, iNKT, ILC1 and ILC3 in tumor. **(B)** Dot plot graphs (left) depict CD11c^{hi}MHCII^{+} cell population in B16 and B16-FL tumors. Floating bars histograms (right) indicate the number of CD11c^{+} MHCII^{+} (DCcont) cells and the total number of Live CD45^{+} cells normalized to 100mg of tumor. The scatter dot plot represents the total tumor weight. **(C)** Total number of cells normalized to 100mg of tumor. **(D-F)** as in (A- C) but in tumor draining lymph nodes (dLN). The numbers in **(E-F)** are not normalized. (n= 5 mice in both B16 and B16FL groups). Student t-tests were performed to compare groups (*: p-value<0.05, **: p-value<0.01, ***: p-value<0.001, ****: p-value<0.0001).

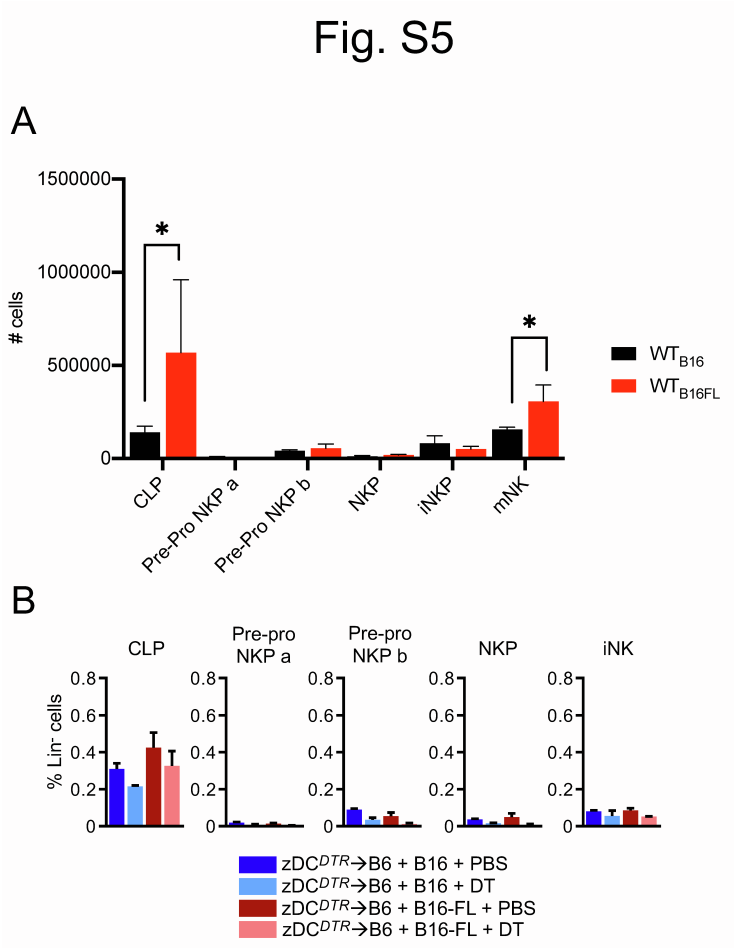

Figure S5. FL overexpression / DC depletion have no major impact on the proportions of NK progenitors in the BM. Related to Figure 5.

(A) Absolute numbers of NK in the bone marrow of the mice from the indicated groups sacrificed at 11 days of tumor growth (n=3-5 mice per group)

(B) Frequencies of several NK precursors in the bone marrow of B16 or B16-FL tumor-bearing *zDC^{DTR}* mice treated with PBS or DT (n=2-6 mice per group).

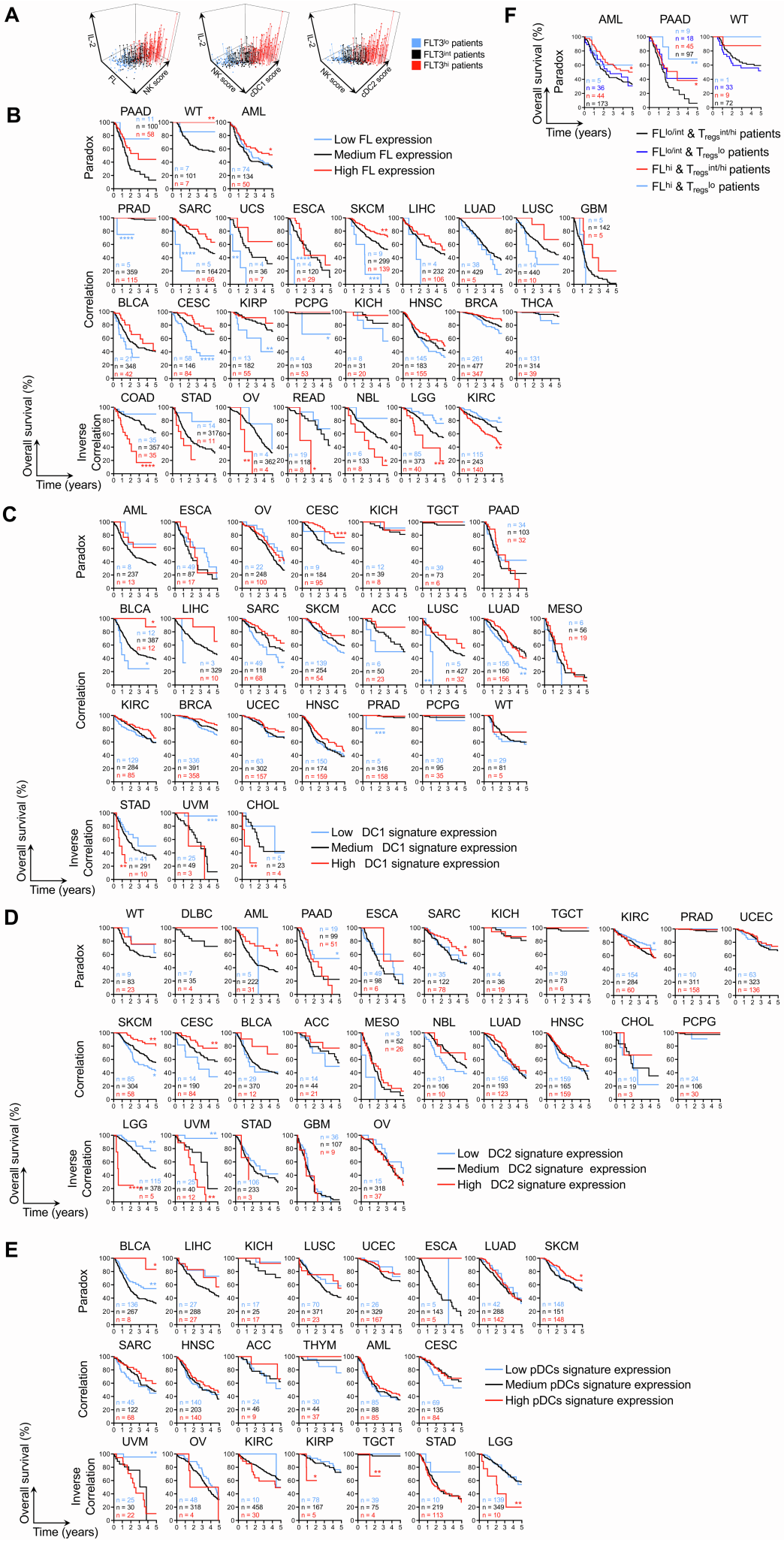
A
IL-2
FL
NK score
cDC1 score
cDC2 score
FLT3lo patients
FLT3int patients
FLT3hi patients
B
PAAD
WT
AML
Paradox
Low FL expression
Medium FL expression
High FL expression
PRAD
SARC
UCS
ESCA
SKCM
LIHC
LUAD
LUSC
GBM
Correlation
BLCA
CESC
KIRP
PCPG
KICH
HNSC
BRCA
THCA
COAD
STAD
OV
READ
NBL
LGG
KIRC
Inverse Correlation
Overall survival (%)
Time (years)
C
AML
ESCA
OV
CESC
KICH
TGCT
PAAD
Paradox
BLCA
LIHC
SARC
SKCM
ACC
LUSC
LUAD
MESO
KIRC
BRCA
UCEC
HNSC
PRAD
PCPG
WT
Correlation
STAD
UVM
CHOL
Inverse Correlation
Low DC1 signature expression
Medium DC1 signature expression
High DC1 signature expression
Overall survival (%)
Time (years)
D
WT
DLBC
AML
PAAD
ESCA
SARC
KICH
TGCT
KIRC
PRAD
UCEC
Paradox
SKCM
CESC
BLCA
ACC
MESO
NBL
LUAD
HNSC
CHOL
PCPG
Correlation
LGG
UVM
STAD
GBM
OV
Inverse Correlation
Low DC2 signature expression
Medium DC2 signature expression
High DC2 signature expression
Overall survival (%)
Time (years)
E
BLCA
LIHC
KICH
LUSC
UCEC
ESCA
LUAD
SKCM
Paradox
SARC
HNSC
ACC
THYM
AML
CESC
Correlation
Low pDCs signature expression
Medium pDCs signature expression
High pDCs signature expression
UVM
OV
KIRC
KIRP
TGCT
STAD
LGG
Inverse Correlation
Overall survival (%)
Time (years)
F
AML
PAAD
WT
Paradox
Overall survival (%)
Time (years)
FLlo/int & Tregsint/hi patients
FLlo/int & Tregslo patients
FLhi & Tregsint/hi patients
FLhi & Tregslo patients

Fig. S6

Figure S6. Effect of FL, DC and Treg transcriptomic gene signatures levels on cancer patient's survival. Related to Figure 6.

(A) *IL2* transcriptomic expression correlates with *FL* expression and with NK, DC1 and DC2 cells signature QS in melanoma patients. 3D graphs show the variations of the indicated parameters for each patient from the SKCM cohort. Each dot represents 1 patient and is colored according to the associated *FLT3* gene expression: *FLT3* low in blue, intermediate in black and high in red.

(B-E) FL and DC1, DC2 and pDC gene signature expression levels have paradoxical effects on patient overall survival in some cancers and are beneficial or detrimental in others. Cancer patients from individual cohorts were classified for *FL* gene or DC-specific gene signature expression. Patients from each cancer type were separated into three groups: low, medium and high according to their expression of *FL* mRNA **(B)**, DC1 **(C)** DC2 **(D)** or pDCs **(E)** gene signatures, and the Kaplan-Meyer graphs show the overall survival of patients for each depicted cancer. Numbers of patients, Log-rank tests p-value comparing low or high groups vs medium group survival are indicated in each graph. **(F)** *FL* gene and Treg signature expressions can synergize to improve patient overall survival in selected types of human cancers. Patients from depicted cancer type were separated into three groups: low, medium and high according to their expression of *FL* gene or Treg gene signature, and the Kaplan-Meyer graphs show the overall survival of patients for each depicted cancer. Numbers of patients, Log-rank tests p-value comparing the different group survival are indicated in each graph (*: p-value<0.05, **: p-value<0.01, ***: p-value<0.001, ****: p-value<0.0001).